RELEASABLE
DOC-CR-CD-89-002

Technical University
of Nova Scotia

Halifax, Nova Scotia
Canada B3J 2X4
Telex: (TUNS) 019-21566

FINAL REPORT ON

"OPTICAL SWITCHING IN A p-i-n DOPED MULTIPLE QUANTUM WELL VERTICAL DIRECTIONAL COUPLER"

Scientific Authority: Dr. Kenneth O. Hill
CRC, Ottawa

Principal Investigator: Dr. Michael Cada
EE-TUNS, Halifax

October, 1990

QC
176.8
O6
C346
1990

IC

FINAL REPORT ON

"OPTICAL SWITCHING IN A p-i-n DOPED MULTIPLE QUANTUM WELL VERTICAL DIRECTIONAL COUPLER"

Industry Canada
Library - Queen
AOUT AUG 2 0 2012
Industrie Canada
Bibliothèque - Queen

Scientific Authority: Dr. Kenneth O. Hill
CRC, Ottawa

Principal Investigator: Dr. Michael Cada
EE-TUNS, Halifax

....

Collaborators: B.P. Keyworth
EE-TUNS, Halifax

J.M. Glinski
C. Rolland
A.J. SpringThorpe
BNR, Ottawa

COMMUNICATIONS CANADA
CRC
NOV 1990
LIBRARY – BIBLIOTHÈQUE

Not to be reported to Aerospace Database.

QC
176.8
O6
C346
1990

D.D. 10258468
D.L. 10270331

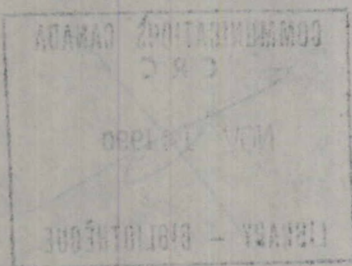

Table of Contents

Introduction ....

1.1 MQW Structures. 2
1.2 Solution to Wave Equation 4
1.3 DC-Biased Quantum Wells 8
1.4 Modelled Characteristics 10
1.5 Relating Absorption to Refractive Index 14

The Linear Directional Coupler. 15

2.1 Phase-Matched Condition. 16
2.2 Mismatched Condition. 17

Theoretical Analysis 17

3.1 Model.bas 18
3.2 Results 19

Experimental Results 25

4.1 Electrooptic Switching 25
4.2 Self-Electrooptic Effect Device 31

Conclusions 38

References 40

Appendix A 44

Table of Figures

Fig. 1 Band structure of a multiple quantum well 3
Fig. 2 DC-biased quantum well 8
Fig. 3 Shift of exciton peak energies versus electric field 11
Fig. 4 Wavefunctions at zero electric field 12
Fig. 5 Wavefunction at an electric field of 50 kV/cm 12
Fig. 6 Wavefunction at an electric field of 100 kV/cm 13
Fig. 7 Decay of resonance peaks versus electric field 14
Fig. 8 Cross section of the vertical directional coupler 18
Fig. 9 Model of the absorption spectra of a MQW. 21
Fig. 10 Refractive index spectra for the MQW layer 23
Fig. 11 Critical coupling length for a linear coupler 24
Fig. 12 Ratio of cross-coupled power to total optical power 25
Fig. 13 Experimental arrangement 26
Fig. 14 Line scans for a sample length of 0.4 mm 27
Fig. 15 Electrooptic switching at bias levels of 5 and 9 V 28
Fig. 16 Wavelength dependency for a 0.4 mm-long sample 29
Fig. 17 Line scans for a sample length of 0.3 mm 30
Fig. 18 Wavelength dependency for a 0.3 mm-long sample 30
Fig. 19 The vertical directional coupler as a SEED device 31
Fig. 20 Output distributions vs. wavelength and applied bias 32
Fig. 21 Switching characteristics predicted by model 33
Fig. 22 Switching achieved with the SEED device 34
Fig. 23 Output distributions for a peak power of 0.65 mW 35
Fig. 24 Intensity distributions for a peak power of 1.38 mW 36
Fig. 25 Waveforms from the generator, AOM, and photodetector 37
Fig. 26 Hysteresis loop 38

Introduction

All-optical switching in a GaAs-based multiple quantum well vertical directional coupler has been demonstrated with coupling lengths as short as 160μm and switching powers of a few milliwatts [1]. Since the lossy multiple quantum well (MQW) layer in this design was used only as a coupling medium between two low-loss waveguides, the device could be operated at wavelengths near the excitonic resonances of the MQW. However, the extinction ratios achievable were limited by saturation of the optical nonlinearity and the switching behaviour was very sensitive to the source wavelength.

In order to overcome these problems the structure was redesigned to operate as an electrooptic switch [2,3]. The mechanism employed in this case was a shift in the absorption spectrum due to electric field known as the quantum-confined Stark effect (QCSE). The strong electroabsorption associated with this effect results in changes in the MQW refractive index which in turn alter the coupling between the two waveguides.

Encouraging results were reported recently for sample lengths of a few hundred micrometers [4]. Much better extinction ratios were achieved (approximately 20:1 as apposed to 4:1 for earlier samples) and switching voltages of only 4 volts were required. In addition, the sensitivity to source wavelength was reduced and a degree of "tuning" capability was supplied by varying the DC bias across the device.

It was expected that an even more robust switching operation could be achieved by configuring the coupler as a self-electrooptic effect device (SEED). The most simple arrangement for a SEED device, which was first conceived by Miller *et al.* for use with quantum well modulators, consists of a reverse biased p-i-n structure in series with a resistor [5]. The resistor provides optoelectronic feedback to the modulator by varying the applied bias voltage in response to changes in photocurrent.

1.1 MQW Structures.

Research on semiconductor superlattices and multiple quantum wells (MQWs) was initiated in 1969 by Esaki and Tsu [6]. In the years since their first proposal for a periodic structure of alternating ultrathin layers, these "engineered" materials have been investigated for a wide variety of device applications [7-16]. These devices include optical modulators, all-optical switches, electro-optic switches, optical logic gates, and bistable devices. The market for these and other devices has been created by the current trend to use lightwaves for telecommunications and high speed computing.

Fabrication of these microstructures became feasible after recent advances in semiconductor growth technology. These advances are a result of the ever increasing demand for integrated electronic devices. Using molecular beam epitaxy (MBE) or metal-organic-chemical-vapour deposition (MOCVD) technique it is now possible to grow semiconductor layers of only a few atomic monolayers. When multiple layers of alternating composition are grown with these dimensions, a new class of materials is developed with completely different characteristics than the bulk materials from which they are comprised.

Much of the research work done to date on MQW structures has concentrated on those consisting of alternating layers of GaAs and AlGaAs. These structures belong to a class of III-V MQW's which are named for the families of elements from which they are comprised. As with all other MQW's, the ultrathin layers are composed of semiconductors with two different band gap energies. The typical band structure of a multiple quantum well is illustrated in Figure 1.

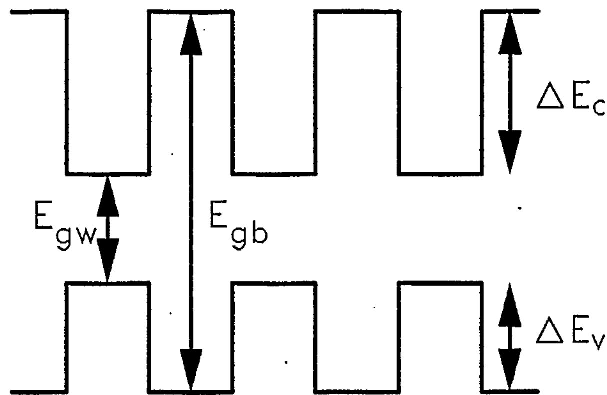

Fig. 1 Band structure of a multiple quantum well.

Here, E_{gb} and E_{gw} are the band-gap energies of the AlGaAs barriers and the GaAs wells, respectively. In the GaAs wells this band-gap energy is 1.424 eV which corresponds to an absorption edge wavelength of 820 nm in the bulk material. For an $Al_xGa_{1-x}As$ material, the band-gap is given by $E_g = 1.424 + 1.247x$ for $0 < x < .45$ or $E_g = 1.9 + .125x + .143x^2$ for $.45 < x < 1$ [17]. The well depths of the conduction band and the valence band are defined by ΔE_c and ΔE_v, respectively. In the early analysis of MQW's, the conduction band was believed to contribute 85 percent to the total well depths while the valence band accounted for the remaining 15 percent. However, more recent work has indicated that these contributions are closer to 60 percent and 40 percent, respectively [18].

Excited electron-hole pairs are confined to the potential wells due to the differences in conduction-band and valence-band energies. The confinement of electrons and holes in the quantum wells creates some distinct differences in the absorption spectra of MQW's and bulk materials. In bulk GaAs, the spectrum exhibits a step like function near the absorption edge with the increase in absorption occuring for $E > E_g$. Therefore, for light with energy less than E_g, there is no generation of electron-hole pairs and

the absorption is relatively low. However, above the absorption edge the light causes generation of free carriers producing an increase in the spectrum.

In quantum well materials the absorption edge is enhanced by one or two resonance peaks due to the presence of loosely bound electron-hole pairs (excitons) in the well material. The wavelengths (or energies) corresponding to these absorption peaks can be obtained from the solution to the Schrodinger wave equation which describes the motion of particles in various force fields.

1.2 Solution to Wave Equation

The general time-dependent Schrodinger equation, which replaces the Newtonian expression $F = ma$ for microscopic phenomena, can be written as:

$$\frac{h^2}{8\pi^2 m}\left(\frac{\partial^2\Psi}{\partial x^2}+\frac{\partial^2\Psi}{\partial y^2}+\frac{\partial^2\Psi}{\partial z^2}\right)-V\Psi=\frac{h}{j2\pi}\frac{\partial\Psi}{\partial t} \quad (1)$$

where h = Plank's constant
m = effective mass
Ψ = wave function
V = potential

If we are dealing with infinite planes in the y & z directions such that

$$\frac{\partial^2\Psi}{\partial y^2} \quad \& \quad \frac{\partial^2\Psi}{\partial z^2} = 0$$

then Eq(1) becomes

$$\frac{\partial^2\Psi(x,t)}{\partial x^2}-\frac{8\pi^2 mV(x)}{h^2}\Psi(x,t)=\frac{4\pi m}{jh}\frac{\partial\Psi(x,t)}{\partial t} \quad (2)$$

Using seperation of variables technique we assume a solution of the form $\Psi(x,t) = \psi(x)\phi(t)$. Substituting into Eq(2) and dividing by $\psi(x)\phi(t)$ we obtain:

$$\frac{1}{\psi(x)}\frac{d^2\psi(x)}{dx^2} - \frac{8\pi^2 mV(x)}{h^2} = \frac{4\pi m}{jh}\frac{1}{\phi(t)}\frac{d\phi(t)}{dt} \tag{3}$$

Since the left hand side of the above equation is a function of x only and the right hand side is a function of t only, then for Eq(3) to be true for all x and t, each side of the expression must be equal to a constant. This constant turns out to be the negative of the total energy of the particle, E.

In modelling the behaviour of MQW materials we are primarily concerned with the spacial variation of Ψ. The time-independent wave equation then reduces to:

$$\frac{d^2\psi}{dx^2} + k^2\psi = 0 \tag{4}$$

where

$$k^2 = \frac{8\pi^2 m}{h^2}(E - V) \tag{5}$$

The solution to Eq(4) is well known and may be expressed in terms of either exponentials or sinusoids.

$$\psi = Ae^{jkx} + Be^{-jkx} \tag{6}$$

or alternatively,

$$\psi = A\sin(kx) + B\cos(kx) \tag{7}$$

where A & B are constants found by applying appropriate boundary conditions.

The most simple problem that may be solved is that of an electron in a potential well with infinitely high walls. Since the electron has finite energy it is not able to penetrate through the potential barriers and will therefore be trapped in the well. Since $|\psi(x)|^2$ in this case represents the probability of finding the electron at a point x, then ψ must be equal to zero at all points outside the well. For a well of width $2a$ the boundary conditions are then $\psi = 0$ at $x = \pm a$. Using Eq(7) this gives,

$$\psi = A\sin(ka) + B\cos(ka) = 0 \qquad ; x = +a \qquad (8)$$

and

$$\psi = -A\sin(ka) + B\cos(ka) = 0 \qquad ; x = -a \qquad (9)$$

For a nontrivial solution we must have either

$$A = 0, \quad \cos(ka) = 0 \qquad or \qquad B = 0, \quad \sin(ka) = 0$$

Taking the second solution yields

$$\psi = A\sin(k_n x) \qquad (10)$$

where

$$k_n = \frac{n\pi}{a} \qquad for \quad n = 1, 2, 3, \ldots$$

Assuming that $V(x)$ is zero inside the well, we obtain the following expression for the "allowed" energies of the electron:

$$E_n = \frac{n^2 h^2}{8ma^2} \qquad n = 1, 2, 3, \ldots \qquad (11)$$

Finally, the constant A is chosen such that

$$\int_{-\infty}^{+\infty} |\psi|^2 \, dx = 1 \tag{12}$$

i.e. the probability of finding the electron somewhere in space is 1.

The above expressions may also be used to calculate the allowed energies of a hole trapped in an infinite potential well by simply changing the effective mass of the particle. In addition, the more practical problem of a potential well with finite barriers can be treated by modifying the boundary conditions so that the wavefunction ψ extends into the barrier regions. In this case the wavevector k will be a real number inside the wells but will become imaginary in the barriers since here $(E-V)<0$. As a result the wavefunctions will be exponentially decaying in the barriers and the boundary conditions will become the continuity of ψ and $d\psi/dx$ at each interface. Furthermore, in a finite potential well the number of discrete energy levels must also be finite since the energy of the particle must be less than the height of the barriers.

The fact that $|\psi|^2 > 0$ outside the well means that there is a finite probability of the particle penetrating the barriers even though the particle energy is less than the barrier height. This phenomenon is known as *tunneling* and has been used to investigate more complicated potential well or quantum well problems [19-21]. In the resonant tunneling technique used in [20], an electron or hole is assumed incident from one side of a potential well and the allowed energies are determined variationally by finding peaks in the transmission coefficient or tunneling current. The technique is applied to quantum well materials under the influence of an applied electric field.

1.3 DC-Biased Quantum Wells

When a multiple quantum well material is exposed to an electric field the conduction and valence bands become tilted. For modelling purposes this can be approximated by a series of potential steps as illustrated in figure 2.

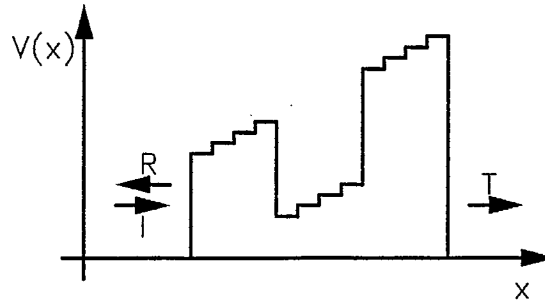

Fig. 2 DC-biased quantum well.

Within each step the wavefunction is assumed to be the combination of a forward and a reverse traveling wave which can be written as:

$$\psi(x) = Ae^{(jkx)} + Be^{(-jkx)} \tag{13}$$

or using the sinusoidal form

$$\psi(x) = \frac{A}{k}\sin(kx) + B\cos(kx) \tag{14}$$

where the wavevector k is as defined in Eq.(5).

Outside the potential well k will be imaginary and the wavefunctions will be exponentially decaying. Substituting $k = j\,|\,k\,|$ into Eq.(14) we obtain the expression for ψ in the barrier regions.

$$\psi(x) = \frac{-jA}{|k|}\sin(j|k|x) + B\cos(j|k|x)$$
$$= \frac{A}{|k|}\sinh(|k|x) + B\cosh(|k|x) \tag{15}$$

The resonant energies which satisfy the Schrodinger equation can now be found by enforcing continuity of ψ and $d\psi/dx$ at each incremental step.

Taking the derivative of Eq.(14):

$$\frac{d\psi}{dx} = \psi'(x) = A\cos(kx) - kB\sin(kx) \tag{16}$$

If we let $x = 0$ then we obtain the values of the constants A & B from equations (14) and (16).

$$A = \psi'(0), \quad B = \psi(0)$$

Therefore over the interval $0 \leq x \leq \Delta x$ we have the complete solution for ψ and ψ' in the potential well:

$$\psi(x) = \frac{\psi'(0)}{k}\sin(kx) + \psi(0)\cos(kx) \tag{17}$$

and

$$\psi'(x) = \psi'(0)\cos(kx) - k\psi(0)\sin(kx) \tag{18}$$

Putting (17) & (18) into matrix form we can derive a transfer matrix which relates the wavefunction at one side of an increment $(x = x_0)$ to that at the other side $(x = x_0 + \Delta x)$.

$$\begin{bmatrix} \psi \\ \psi' \end{bmatrix}_{x=x_0+\Delta x} = \begin{bmatrix} \cos(kx) & (1/k)\sin(kx) \\ -k\sin(kx) & \cos(kx) \end{bmatrix} \begin{bmatrix} \psi \\ \psi' \end{bmatrix}_{x=x_0} \tag{19}$$

If the wavevector k is imaginary then Eq.(19) becomes:

$$\begin{bmatrix} \psi \\ \psi' \end{bmatrix}_{x=x_0+\Delta x} = \begin{bmatrix} \cosh(|k|x) & (1/|k|)\sinh(|k|x) \\ |k|\sinh(|k|x) & \cosh(|k|x) \end{bmatrix} \begin{bmatrix} \psi \\ \psi' \end{bmatrix}_{x=x_0} \quad (20)$$

Using these transfer matrices we can compute the electron and hole wavefunctions across the well and barriers. The energy of the incident particle is then varied until a resonance is found in the transmission coefficient corresponding to a resonance energy $E = E_n$.

1.4 Modelled Characteristics

For a GaAs/AlGaAs multiple quantum well three resonance energies must be computed, E_c, E_{hh}, and E_{lh}. These correspond to the electron, heavy hole, and light hole, respectively. In each case the appropriate effective mass and barrier potential must be used in determining the wavevector. The subband gaps for the heavy and light hole are then given by:

$$E_{e-hh} = E_g + E_c + E_{hh} - E_{bind} \quad (21)$$

and

$$E_{e-lh} = E_g + E_c + E_{lh} - E_{bind} - E_{strn} \quad (22)$$

where E_g is the bandgap of the GaAs wells, E_{strn} is a strain shift created during fabrication of the sample, and E_{bind} is the exciton binding energy. The strain shift is negligible for heavy holes but accounts for approximately 4.5 meV in the light hole case [21]. Typical values for the binding energy are 7 and 8 meV for heavy and light holes respectively. These values vary somewhat with electric field but for our purposes we will assume they are constant. This seems justified since variational methods must be used to determine their exact values and the perturbation that would be introduced is small [21].

Typical calculated values for E_{e-hh} and E_{e-lh} are illustrated in figure 3 for a well width of 10 nm in electric fields of 0 to 100 kV/cm. It can be seen that for increasing electric fields the subband gaps are shifted towards lower energies.

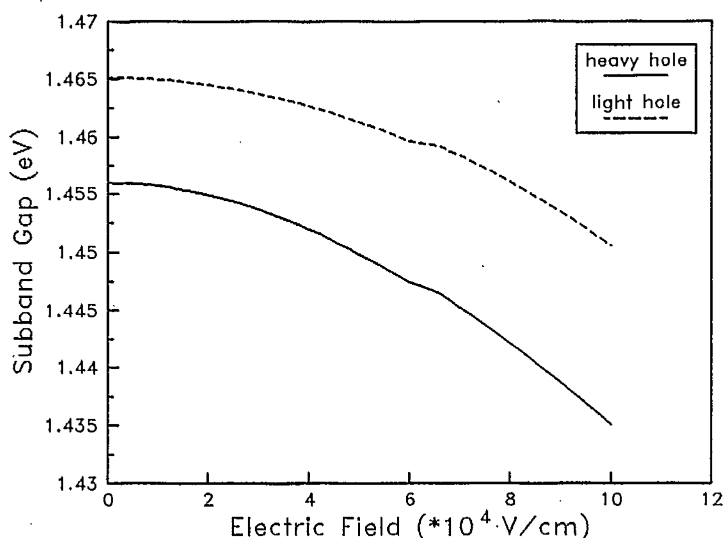

Fig. 3 Shift of exciton peak energies versus electric field.

The shifts observed in figure 3 for increasing electric fields are due to the bound electron-hole pairs being pulled to opposite sides of the wells thus reducing the coulomb attraction between them. This is known as the quantum-confined Stark effect (QCSE) and is the dominant mechanism involved in electroabsorption and electrorefraction in quantum wells. The pulling apart of the electrons and holes can be seen from the wavefunctions depicted in figures 4-6 for electric fields of 0, 50, and 100 kV/cm, respectively. The amplitude of each wave function is normalized so that the integral of ψ^2 over all x is equal to one.

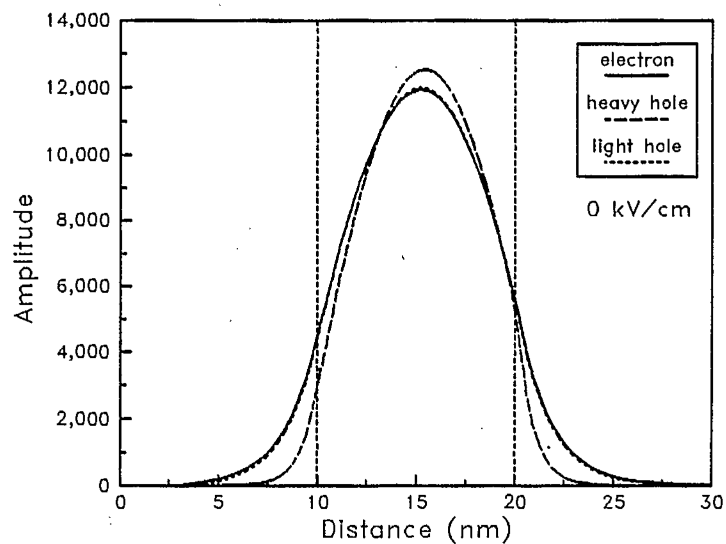

Fig. 4 Wavefunctions at zero electric field.

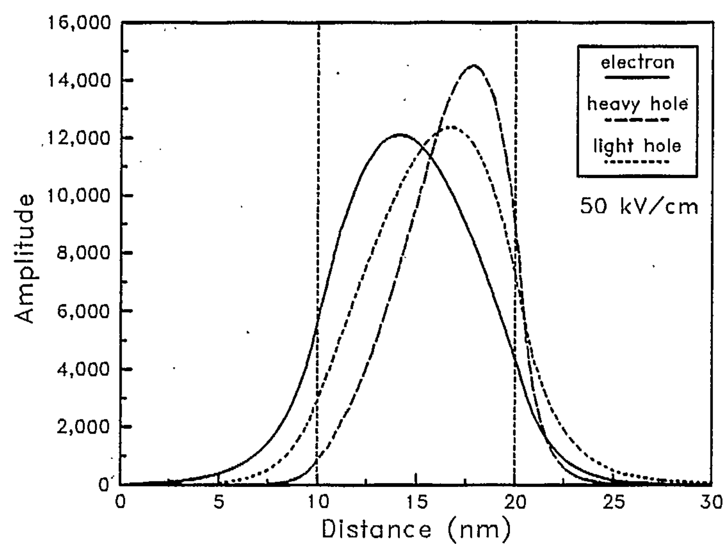

Fig. 5 Wavefunctions at an electric field of 50 kV/cm.

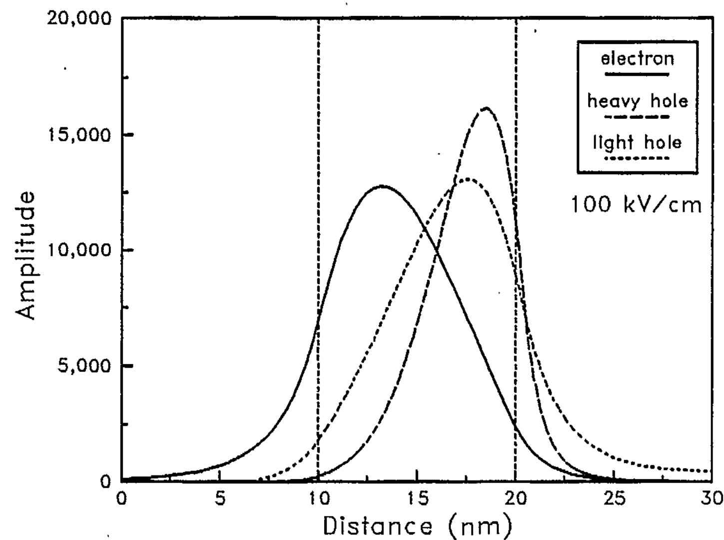

Fig. 6 Wavefunctions at an electric field of 100 kV/cm.

From the above wavefunctions we can see that an increasing electric field causes a reduction in the overlap integral of the electron and holes, which is defined as:

$$M_{e-h} = \left| \int_{-\infty}^{\infty} \psi_e(x)\psi_h(x)dx \right| \tag{23}$$

It has been demonstrated that the strengths of the exciton resonance peaks in MQWs are proportional to the square of the overlap integrals [22]. The oscillator strengths versus electric field are plotted in figure 7.

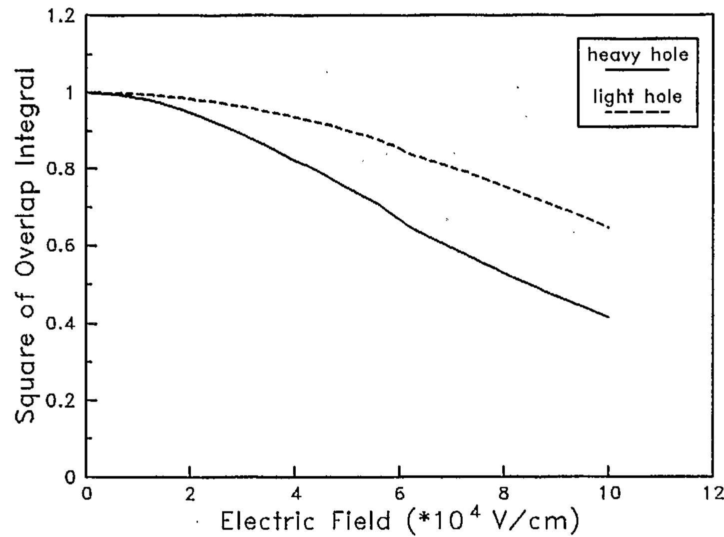

Fig. 7 Decay of resonance peaks versus electric field.

1.5 Relating Absorption to Refractive Index

Due to the resonance peaks in the absorption spectrum, the effective absorption coefficient of MQW materials is altered by the presence of excitons. These changes in absorption can be related through the Kramers-Kronig relation to changes in effective refractive index of the MQW layer [23] :

$$\Delta n(\omega) = \frac{c}{\pi} P \int_0^{\infty} \frac{\Delta \alpha(\omega')}{\omega'^2 - \omega^2} d\omega' \qquad (24)$$

In qualitative terms, the changes can be related by considering the interaction of incident photons with those emitted through electron-hole recombination. If the incident radiation is of an energy near or above the bandgap of the semiconductor, then photons will be absorbed and electron-hole pairs will be generated. After a certain period, the mean carrier lifetime, recombination will take place. The energy released from the recombination will in some cases be absorbed in heating of the crystal while in other cases will involve the emission of a photon of the same wavelength as the incident one. In the latter case, the emitted photon may

not have the same phase as the incident field. The effect is to change the phase velocity of the incident wave or equivalently, change the refractive index.

At wavelengths near the resonance peaks, excitons are generated and are then ionized by thermal phonons into free-carriers. At room temperature the exciton lifetime has been measured to be approximately 0.5 ps [24]. At high intensities the Coulomb interaction associated with the excitons is screened by the free carriers. Thus the excitonic absorption saturates and the resonance peaks eventually disappear. The effects induced by free carriers will be present until the electrons and holes recombine. This is a much slower process with lifetimes found to be approximately 10 ns.

The Linear Directional Coupler.

When two identical waveguides are placed in close proximity and the input of one waveguide is excited with optical energy, the power will transfer periodically between the two waveguides as the light propagates down the structure. The distance required for a full transfer of power from one waveguide to the other is referred to as the critical coupling length, L_c, and is a function of the refractive index profile across the two guides and the spacing between them.

The operation of the directional coupler can be described analytically using the coupled-mode equations [25] :

$$\frac{da_A}{dz} = -jC_{BA}e^{j\Delta kz}a_B(z) \tag{25}$$

$$\frac{da_B}{dz} = -jC_{AB}e^{j\Delta kz}a_A(z) \tag{26}$$

where

$$\Delta k = k_{ZA} - k_{ZB}$$

$$a_{A,B}(z) = a^0_{A,B}e^{-j\gamma_{A,B}z}$$

In the above expressions, a_A and a_B are the normalized amplitudes in guide A and B, respectively. C_{AB} and C_{BA} are coupling coefficients.

If all of the input power is incident on guide B at the input so that $a_A(0) = 0$, then the power in each waveguide as a function of z is given by:

$$P_A(z) = |a_A(z)|^2 = P_0 \frac{|C_{BA}|^2}{S^2} \sin^2(Sz) \tag{27}$$

$$P_B(z) = |a_B(z)|^2 = P_0 \left[\left(\frac{\Delta k}{2S} \right)^2 \sin^2(Sz) + \cos^2(Sz) \right] \tag{28}$$

where

$$S = \sqrt{\left(\frac{\Delta k}{2} \right)^2 + C_{BA} C_{AB}} \tag{29}$$

$$P_0 = \frac{(2A)^2}{|C_{BA}|^2} S^2 \tag{30}$$

and A is an arbitrary constant.

2.1 Phase-Matched Condition.

If waveguides A and B are truly identical then the propagation constants are also identical and $\Delta k = 0$. Therefore, under phase-matched conditions we have $C_{AB} = C_{BA} = C$ and we obtain :

$$P_A(z) = P_0 \sin^2(Cz) \tag{31}$$

$$P_B(z) = P_0 \cos^2(Cz) \tag{32}$$

The propagation length required for a full transfer of power is given by:

$$\sin(CL_c) = 1 \tag{33}$$

$$or \qquad L_c = \frac{\pi}{2C} \tag{34}$$

Note that as the coupling between the waveguides is increased, the full-transfer length is reduced.

2.2 Mismatched Condition.

If the waveguides in the directional coupler are not identical ($\Delta k \neq 0$), the maximum power transferred to guide A occurs at $z = \pi/2S$. In this case we have :

$$\left(\frac{P_A}{P_0}\right)_{\max} = \frac{|C_{BA}|^2}{C_{AB}C_{BA} + \frac{\Delta k^2}{4}} \qquad (35)$$

and a complete transfer of power from guide A to guide B cannot occur.

Theoretical Analysis

In the nonlinear directional coupler discussed here, a GaAs-based MQW is used as a coupling medium between two slab waveguides. The critical coupling length of the device is therefore dependent on the refractive index of the MQW layer. Thus the QCSE can be employed as a switching mechanism to vary the output distribution of the optical beam.

The structure is illustrated in figure 8. The two $Al_{.15}Ga_{.85}As$ waveguides are 1.85 μm thick and are buffered from above and below by 2 μm $Al_{.60}Ga_{.40}As$ layers. The multiple quantum well layer consists of 30 periods of 9.6 nm GaAs wells and 21 nm $Al_{.33}Ga_{.67}As$ barriers, for a total thickness of approximately 0.9 μm. Dopants were added to the materials to form a p-i-n structure with the MQW layer acting as the intrinsic region. A gold layer was deposited on the top surface of the structure which is then bonded to a copper holder with a metallic epoxy.

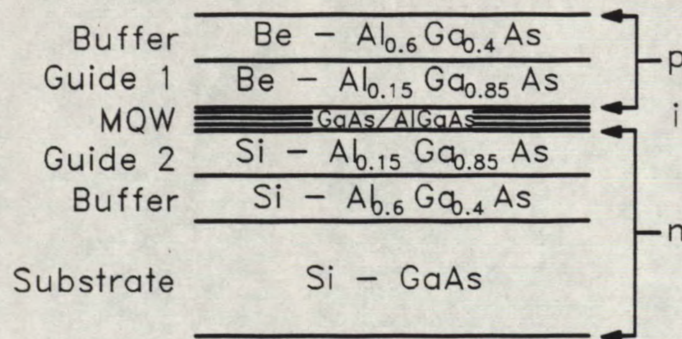

Fig. 8 Cross-section of the vertical directional coupler. Thicknesses of the waveguides, buffers, and MQW are 1.8 μm, 2 μm, and 0.9 μm, respectively.

3.1 Model.bas

A listing of the program MODEL.BAS can be found in Appendix A. This is the main program used in analyzing the vertical directional coupler under various applied electric fields.

The series of steps performed by the program are as follows:

1. Calculate the exciton resonance wavelengths for zero bias and for a user specified voltage.

2. Compute the electron, light-hole, and heavy-hole wavefunctions for each bias voltage and then determine the overlap integrals.

3. Calculate the zero bias absorption spectrum and the shifted spectrum for the specified voltage. Plot the spectra and calculate the differential absorption.

4. Determine the differential refractive index using the Kramers -Kronig transformation and add this to the zero bias case. Plot both differential absorption and differential refractive index.

5. Using the total refractive index spectrum, determine the critical coupling length of the directional coupler by first calculating the propagation constant of the fundamental mode and then finding coupling coefficient K.

6. Finally, calculate the ratio of cross-coupled power to total power for a fixed length coupler which varies as $\sin^2(KL)$. Plot the cross-coupling on the screen and then save all calculated curves in a data file.

3.2 Results

In the program MODEL.BAS, a model of the absorption spectrum reported in [26] was used along with the Kramers-Kronig transformation to obtain the refractive index of the MQW. The model assumes Gaussian lineshapes for both the heavy hole and light hole excitonic resonances along with a broadened continuum. The resulting expression is as follows:

$$\alpha(\hbar\omega) = \alpha_h \exp\left[-\frac{(\hbar\omega - \hbar\Omega_h)^2}{2(\hbar\Gamma_h)^2}\right] + \alpha_l \exp\left[-\frac{(\hbar\omega - \hbar\Omega_l)^2}{2(\hbar\Gamma_l)^2}\right] \quad (36)$$

$$+ \frac{2\alpha_c}{\left[1 + \exp\left(\frac{\hbar\Omega_c - \hbar\omega}{\hbar\Gamma_c}\right)\right]\left[1 + \exp(-2\pi[|\hbar\Omega_c - \hbar\omega|/R_y]^{-1/2})\right]} \quad (37)$$

where $\hbar\omega$ is the incident photon energy, $\hbar\Omega_h$ & $\hbar\Omega_l$ are the heavy-hole and light-hole peak energies, and $\hbar\Omega_c$ is the energy of the continuum edge. The terms $\hbar\Gamma_h$, $\hbar\Gamma_l$, and $\hbar\Gamma_c$ represent the half linewidths of each contribution while R_y is the Rydberg constant of the material. Typical values of these parameters along with the amplitudes α_h, α_l, and α_c are shown in table 1.

Parameter	0 volts	5 volts	9 volts
α_h (10^3/cm)	11.500	6.4688	2.5674
α_l (10^3/cm)	6.000	4.8600	2.9400
α_c (10^3/cm)	3.800	3.8000	3.8000
$\hbar\Omega_h$ (eV)	1.457	1.4500	1.4390
$\hbar\Omega_l$ (eV)	1.466	1.4615	1.4540
$\hbar\Omega_c$ (eV)	1.466	1.4660	1.4660
$\hbar\Gamma_h$ (meV)	3.000	4.0000	6.2000
$\hbar\Gamma_l$ (meV)	3.000	4.0000	6.2000
$\hbar\Gamma_c$ (meV)	5.000	6.0000	8.2000

Table 1 Parameters used to obtain the absorption spectra shown in the following figure.

Accurate experimental measurements of the absorption spectra cannot be obtained for our structure since the changes in MQW refractive index associated with the electroabsorption create variations in the waveguide numerical aperture and hence the launched optical power. The zero bias amplitudes and linewidths in table 1 were therefore chosen by comparing results reported in the literature for similar MQW structures [19,21,22]. The shifts, decay, and spreading of the excitonic resonances for non-zero electric field were computed by the program as were the zero bias subband gaps. The resulting spectra are shown in figure 9 for applied bias levels of 0, 5, and 9 volts.

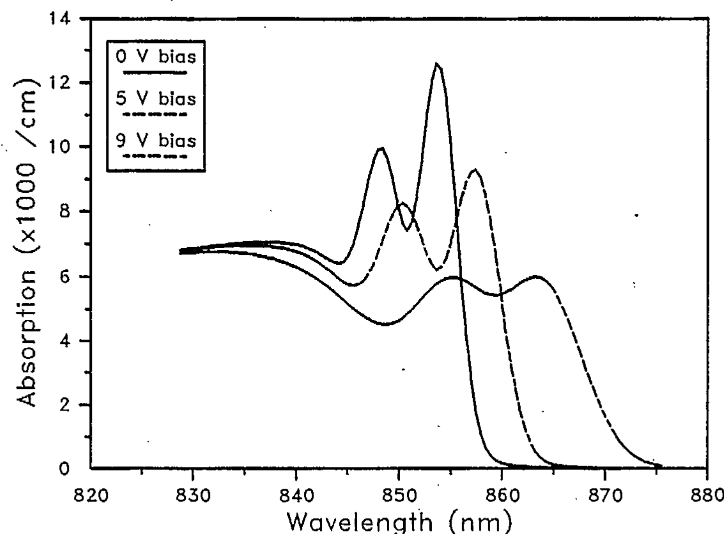

Fig. 9 Model of absorption spectra for a GaAs/AlGaAs MQW under several reverse bias conditions.

The absorption spectra above agree very closely to reported experimental results with the exception of one area in the continuum. It can be seen in the figure that the model predicts a dip in the absorption at wavelengths just below the light-hole peak. This feature becomes more prominent as the applied electric field is increased but in actual fact is not observed in the experimental data. The source of this discrepency is believed to be the N=1 electron to N=2 heavy-hole transition which will increase in strength with electric field. At present the model does not include this transition but it will be added in future versions. The dip should then be "filled in" by the higher order transition and a better experimental fit should be obtained. A simpler way to overcome the problem is to assume the continuum edge shifts with the light-hole resonance. This was done in earlier models [4] but the effect on the predicted switching characteristics was surprisingly small.

The effective refractive index for the zero bias case is derived by adding a constant background term to the excitonic contribution calculated, using the Kramers-Kronig relation, from the difference between the saturated and nonsaturated absorption spectra. The background term is estimated using the expression below [27]:

$$n_{rms}^2 = \frac{L_a n_a^2 + L_b n_b^2}{L_a + L_b} \qquad (38)$$

where subscripts a and b denote well and barrier, respectively. The bulk refractive indices used for the GaAs wells and $Al_{.33}Ga_{.67}As$ barriers are 3.63 and 3.486 [17], leading to an rms value of 3.5317 for the MQW layer. The changes in refractive index when an electric field is applied perpendicular to the wells are obtained from the differential absorption spectrum and are then added to the zero field values. The resulting curves for the refractive index of the MQW under bias conditions of 0, 5, and 9 volts, are plotted in figure 10. For an effective directional coupler, the refractive index of the coupling layer must be close to that of the waveguides (3.565 in this case). Therefore, referring to figure 10, there are three regions which will yield strong cross-coupling. These are; 855nm for 0 V bias, 860 nm for 5 V bias, and 865 nm for 9 V bias. At all other areas on the curves the refractive index of the MQW decreases and the waveguides become decoupled.

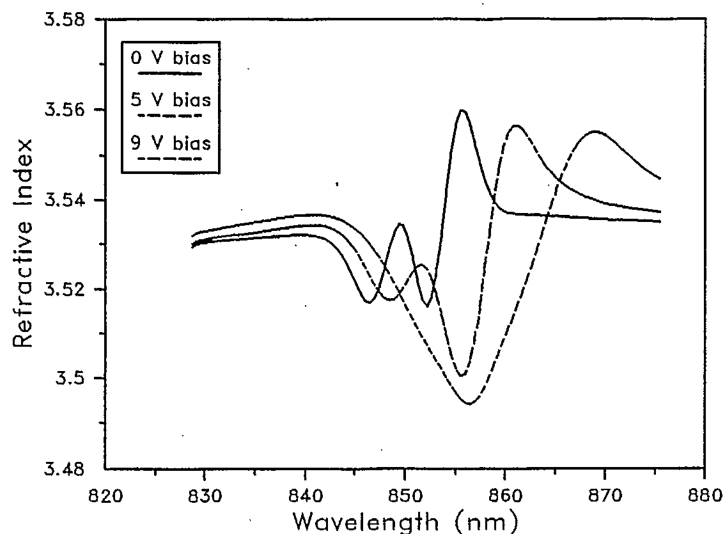

Fig. 10 Refractive index spectra for the MQW layer under the same three bias conditions.

Once the refractive index of the MQW coupling layer has been evaluated, the critical coupling length of the device can be determined. Since the model used here is approximate and the optical intensity levels used in the experiments are low, we assume the coupler is a linear device and calculate the coupling coefficient K. The fraction of cross-coupled power is then given by:

$$\frac{P_{coupled}}{P_{total}} = \sin^2(\mathrm{K}L) \tag{39}$$

The results of this analysis are shown in figures 11 and 12. From the first figure we can see that for each bias level there is a minimum coupling length of approximately 300-400 μm. However what is interesting to note is that the wavelength at which the minimum occurs is shifted further into the infrared as the voltage is increased. For instance, in the zero bias case the minimum coupling length occurs at 855 nm and when a bias of 5 volts is applied it is shifted to 860 nm.

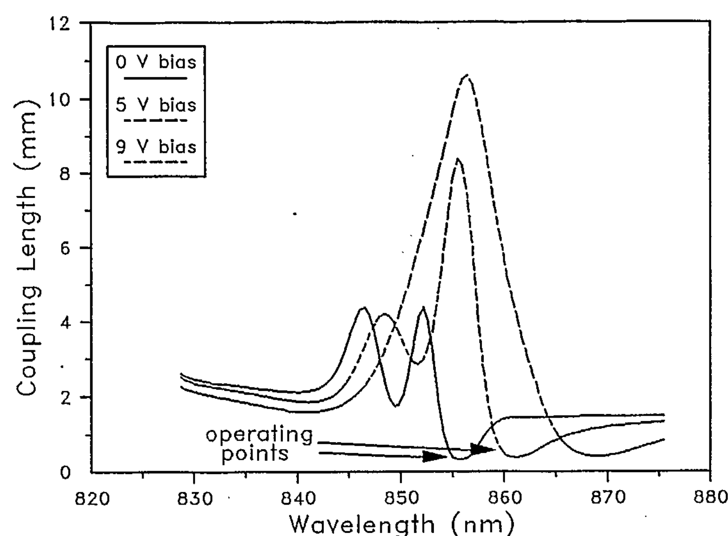

Fig. 11 Critical coupling length for a linear directional coupler with the refractive index of the coupling layer determined from the absorption spectra of figure 9.

In figure 12 the predicted cross-coupling for a 400-μm sample is plotted for the same three bias levels. The slight dip at 855 nm for the zero bias case occurs because the critical coupling length reaches values below 400 μm. The model shows that at 860 nm the output distribution of the coupler should vary from approximately 15 % in the crossed waveguide at 0 volts, to 95 % at 5 volts, and then back down to 4 % at 9 volts bias. It should also be noted that in figure 9 there is a point near 860 nm which yields a large increase in absorption between 0 and 5 volts bias, with no change in absorption between 5 and 9 volts. In addition, there is a second point near 855 nm in figure 9 where all three bias levels produce approximately the same absorption, while at the same wavelength the curves in figure 12 show that a strong switching should occur between 0 and 5 volts.

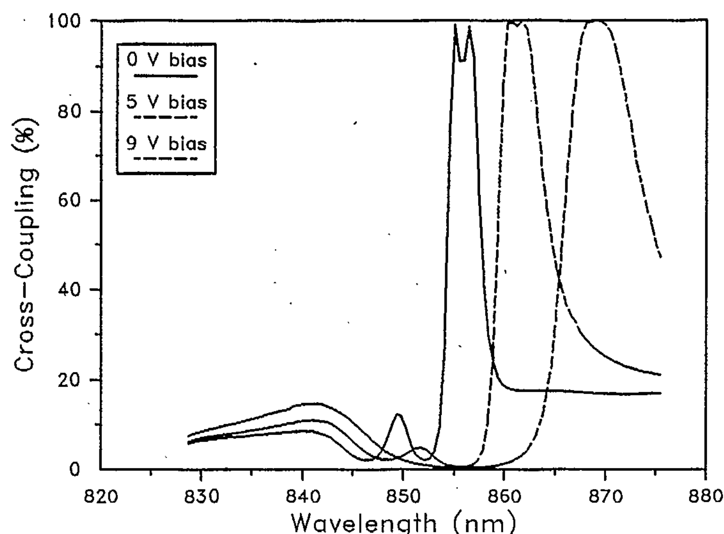

Fig. 12 Ratio of cross-coupled power to total optical power for a sample length of 400μm.

Experimental Results

4.1 Electrooptic Switching

From the model of the p-i-n doped structure it was expected that the voltage levels required for switching should be less than 10 volts. Since all layers other than the MQW are doped, a 10 volt bias would correspond to an electric field strength in the order of 10 V/μm ($1x10^5$ V/cm). Previous work by several authors has illustrated significant shifts in the absorption spectra at this field strength [19,21,22].

The experimental arrangement used in testing the couplers is shown in figure 13. An Argon-pumped, Styryl-9 dye laser was employed as the light source which is end-fire coupled to the samples through a microscope objective lens. Selection of a TE or TM mode was achieved by rotating the half-wave plate located in front of the sample. An electric field was created over the entire length of the coupler by applying a voltage between the top gold layer and the copper holder on the bottom.

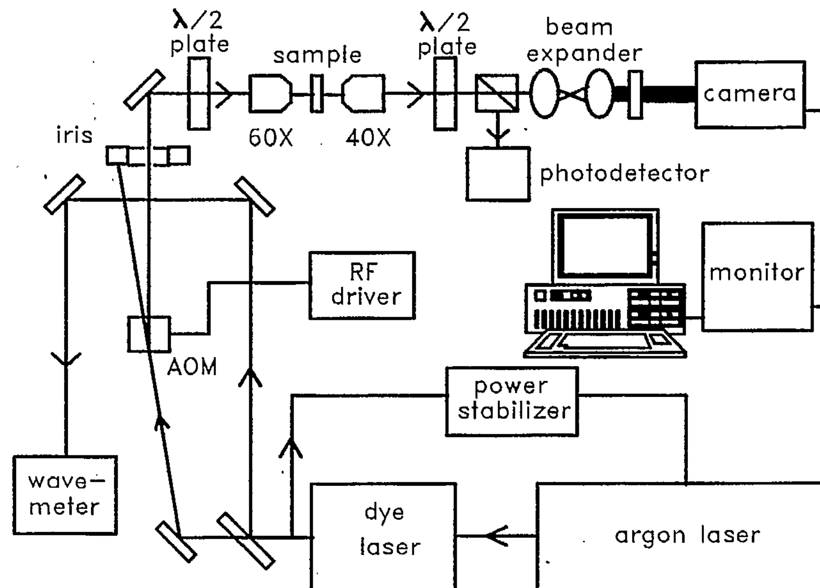

Fig. 13 Experimental arrangement used in testing the electrooptic switching elements.

At the output of the device, the intensity distribution between the two waveguides was monitored with an infra-red camera and/or a photodetector. Line scans were obtained from the camera by digitizing a frame of video for analysis on a personal computer. Due to the automatic gain control circuitry of the camera, however, absolute changes in intensity could not be detected. Therefore, a photodetector with a fiber pigtail was used for this purpose. In order to observe the field pattern with the photodetector, the fiber pigtail was scanned through the output beam.

The electrooptic switching achieved with a sample length of 400μm is illustrated in figure 14. In order to avoid nonlinear optical effects, a low incident power of 0.1 mW is used. The wavelength of operation is 860 nm, approximately 7 nm above the heavy hole exciton peak. A TE mode is launched in the top waveguide which appears on the right side of the figure. It can be seen that as the bias voltage is increased from 0 to 9 volts the output distribution shifts from the bar state to the crossed state and back

again. It should be noted that these intensity scans are taken from the infrared camera and are therefore normalized independently. By scanning the photodetector through the beam it was found that while there was a large difference in the peak intensity between the zero bias and the 5 volt case, the intensity remains virtually equal when alternating between 5 and 9 volts. In fact the change in peak intensity is only 2.5 % between the latter two bias levels yet a near-complete transfer from the crossed state to the bar state is achieved. A result of such a scan is shown in figure 15. In this case there must be a significant drop in the refractive index of the MQW which occurs with no change in absorption.

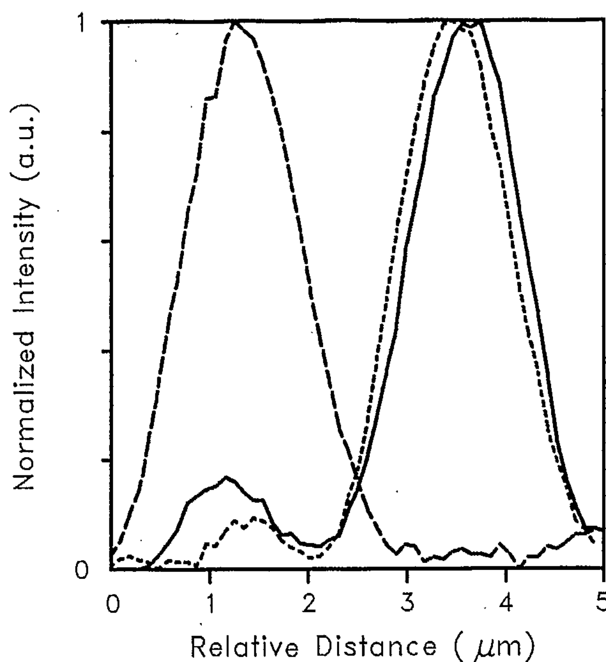

Fig. 14 Line scans from an infrared camera for a sample length of 400 μm. Incident optical power is 0.1 mW at a wavelength of 860 nm. Solid curve - zero bias, dashed curve - 5 V bias, dotted curve - 9 V bias.

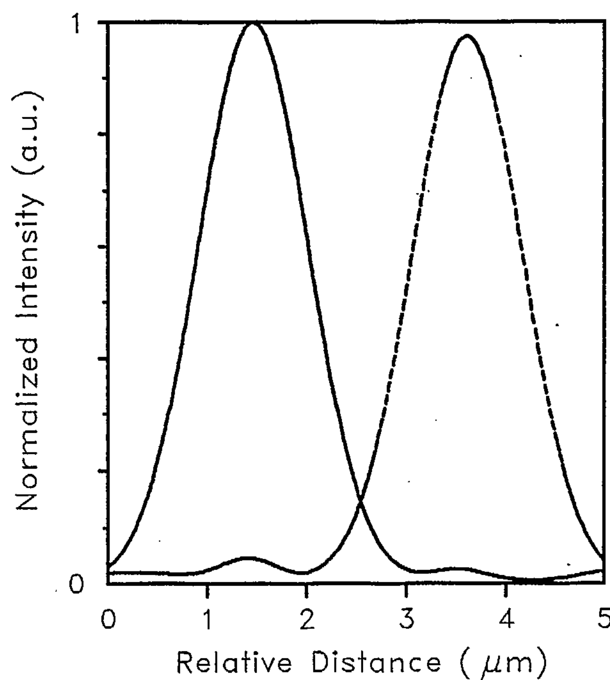

Fig. 15 Electrooptic switching between bias levels of 5 V and 9 V. Line scans are obtained using a fiber pigtailed photodetector. Solid curve - 5 V bias, dashed curve - 9 V bias.

Since it is believed that the mechanism responsible for this switching is a shift in the absorption spectrum brought on by the QCSE, a similar operation should be achieved by manually tuning the wavelength of the laser light source. This was verified in the experiments and the results for the 400μm sample are shown in figure 16. It can be seen that at the wavelengths of 860.5 nm, 854.5 nm, and 846.5 nm, the output distributions correspond roughly to those at zero bias, 5 V bias, and 9 V bias in figure 14.

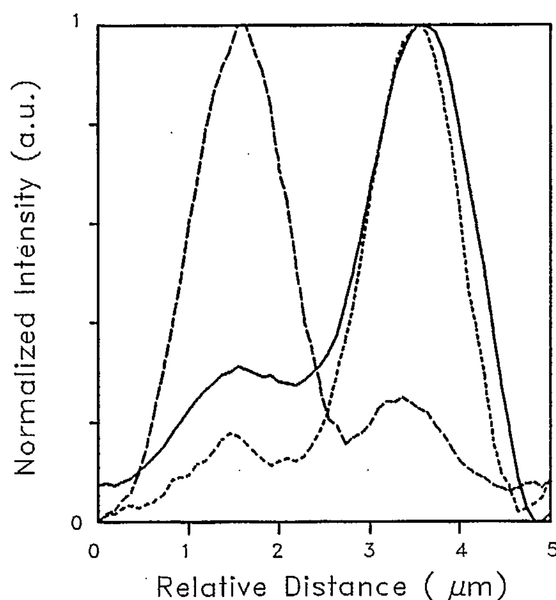

Fig. 16 Wavelength dependency of the output distribution from a 400 μm-long sample. Solid curve - 860.5 nm, dashed curve - 854.5 nm, dotted curve - 846.5 nm.

The experiments were repeated with a second sample which was cleaved to a length of 300 μm. However, in this case the wavelength for electrooptic switching was chosen closer to the absorption peak where a cross-coupled condition is achieved at zero bias. It was found that an applied reverse voltage of 5 volts was enough to produce switching from the crossed to the bar state. Again, the intensity between these two cases remained virtually constant, indicating no change in the absorption coefficient. This switching operation along with that obtained by manually tuning the wavelength are illustrated in figures 17 and 18.

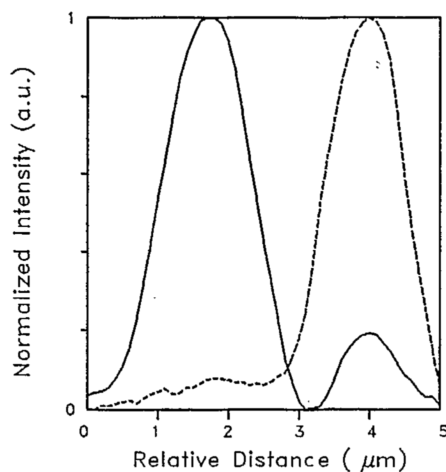

Fig. 17 Line scans from an infrared camera for a sample length of 300 μm. Incident optical power is 0.1 mW at a wavelength of 855 nm. Solid curve - zero bias, dashed curve - 5 V bias.

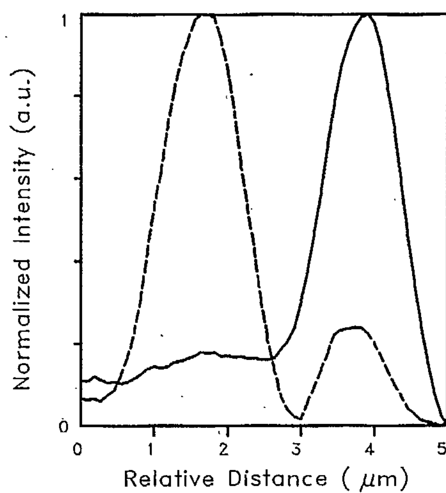

Fig. 18 Wavelength dependency of the output distribution from a 300 μm-long sample. Solid curve - 855.2 nm, dashed curve - 848.5 nm

4.2 Self-Electrooptic Effect Device

It was expected that an even more robust switching operation could be achieved by configuring the coupler as a self-electrooptic effect device (SEED). The most simple arrangement for a SEED device, which was first conceived by Miller *et al.* for use with quantum well modulators, consists of a reverse biased p-i-n structure in series with a resistor [5]. The resistor provides optoelectronic feedback to the modulator by varying the applied bias voltage in response to changes in photocurrent. For example, if the device is operated at wavelengths near the zero field absorption peak of the quantum wells, then at low optical powers the reverse bias will shift the spectrum and absorption will be low. As the incident optical power is increased, the resulting photocurrent produces a voltage drop across the resistor which reduces the bias on the modulator. The device is therefore shifted back towards the high absorption state.

By configuring the directional coupler as a SEED, control of the switching operation is returned to the optical beam itself rather than an electrical signal. However, the improved performance associated with the quantum-confined Stark effect is maintained. The simplest arrangement of a resistor in series with the reverse biased coupler was employed as illustrated in Figure 19.

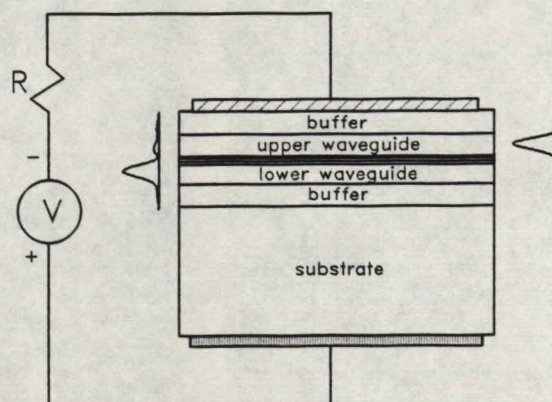

Fig. 19 The vertical directional coupler configured as a SEED device.

The output intensity distribution from a sample cleaved to 250 μm is shown in Figure 20 for several combinations of wavelength and electric field. No external feedback resistor was used in this case so there are no self-electrooptic effects. The incident light is coupled into the top (right) waveguide and a low power level is used in order to avoid nonlinear optical effects.

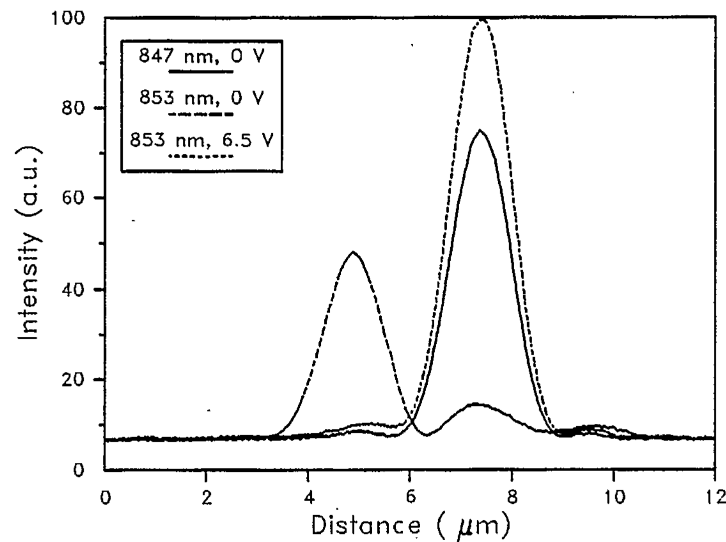

Fig. 20 Output distributions for several combinations of wavelength and applied bias.

It can be seen that as the source wavelength is varied from 847 nm to 853 nm, the zero field output distribution shifts from the bar to the crossed state. If the bias voltage is then increased to 6.5 volts, which corresponds to an electric field of approximately 65 kV/cm, then a red shift in the absorption spectrum causes the distribution to switch back to the bar state. The increased ouput power in this case, over that at 847 nm, can be attributed to the decay in the absorption peaks as the spectrum is shifted and/or the fact that the shift is not exactly 6 nm.

Figure 21 shows the predictions from the model of the coupler.

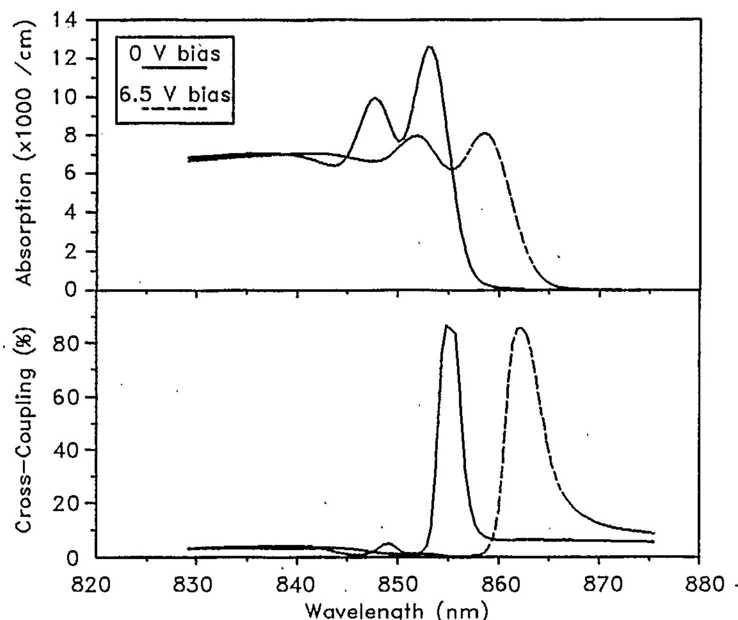

Fig. 21 Switching characteristics predicted by the computer model

Comparing the experimental results to the predicted behaviour we can see a good correlation. Strong electrooptic switching is evident at wavelengths near 855 nm with relatively small changes in absorption. In addition, tuning the source wavelength away from 855 nm causes the distribution to switch from the crossed to the bar state at zero bias.

The experimental results obtained with the 250 μm-long sample configured as a SEED are shown in Figure 22. Again the incident light is coupled to the top (right) waveguide and the source wavelength in this case is 854 nm. The external components consist of a 7 volt fixed bias and a 10 kΩ feedback resistor. At this wavelength the output distribution would be in the crossed state for zero electric field. However, at low optical powers the 7 volt bias shifts the absorption spectrum of the MQW through the QCSE and the switch is therefore in the bar condition. As with the SEED modulators described previously, when the incident power is increased the

resulting photocurrent produces a voltage drop across the resistor which reduces the bias on the device. The coupler then switches to the crossed state as the electric field in the MQW layer reduces to zero.

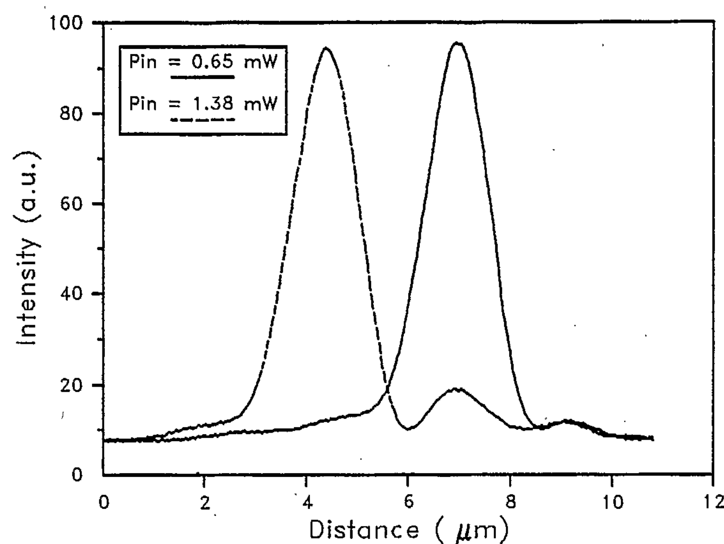

Fig. 22 Switching achieved with the coupler configured as a SEED device.

With the 10 kΩ resistor in the feedback loop the switching threshold was at an incident optical power of approximately 1 mW. This produced a bar condition at 0.65 mW and a crossed condition at 1.38 mW, as seen in the figure. However, the threshold power can be varied over a wide range by suitable choice of the resistor. It is expected that the upper power limit would be governed by thermal effects while the lower limit would be due to leakage current of the device. It is also possible to choose the source wavelength over a range of values above 853 nm and compensate for the deviation by increasing the bias voltage. This is evident in the case described above as the bias voltage was increased from 6.5 to 7 volts in order to compensate for a wavelength of 854 nm.

An interesting point to note is that although the input optical power is approximately doubled in order to switch from one waveguide to the other, the output power remains constant. This is due to the difference in absorption between the zero bias case and that at 6.5 volts, which offsets the increasing power. Refering to Figure 21, it can be seen that at a wavelength of 853 nm, the peak intensity for the zero bias case is only half that at 6.5 volts bias. Thus when the input optical power is doubled in order to reduce the voltage across the SEED device to zero, the output powers become equal.

In order to verify that no thermal effects were involved in the operation of the SEED, experiments were conducted using a modulated source. It was found that the duty cycle of the incident light could be varied from 96% down to 6 % and the output distribution for peak powers of 0.65 and 1.38 mW remained exactly the same as with the continuous wave source. This is illustrated in Figures 23 and 24.

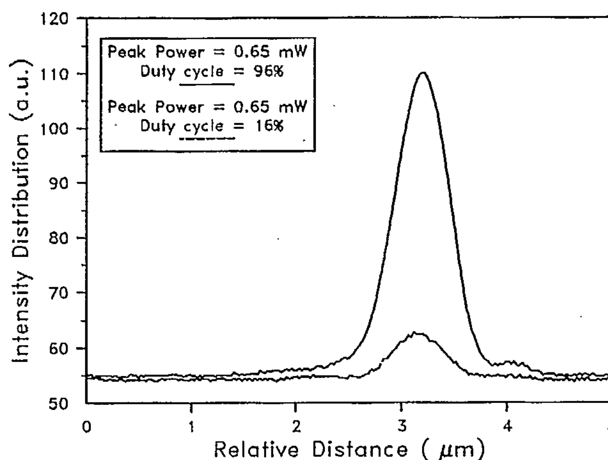

Fig. 23 Intensity distributions for a peak power of 0.65 mW with duty cycles of 96% and 16%.

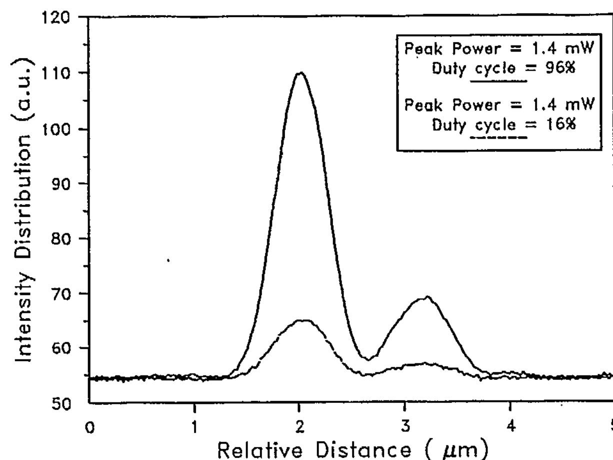

Fig. 24 Intensity distributions for a peak power of 1.38 mW with duty cycles of 96% and 16%.

Further confirmation was supplied by the ability to change the switching threshold of the coupler by changing the feedback resistor. If thermal effects were responsible for the switching, this would not have been possible.

One final characteristic of SEED devices which is worth consideration is the bistability observed in the absorption. This has been reported in [5] for SEED modulators but to our knowledge has not been investigated in coupling devices. The bistability is evident when operating at wavelengths near the zero bias absorption peaks of the MQW. At low optical powers the full bias voltage is applied to the device and the absorption peak is shifted to longer wavelengths. As the input power is increased the resulting photocurrent produces a voltage drop across the resistor and the bias across the device is therefore decreased. This causes the absorption spectrum to be shifted back toward the high absorption state which in turn generates more photocurrent, etc.

Since the absorption, refractive index, and coupling length in a directional coupler are all interrelated, the bistability takes on a new significance. If two possible absorption states exist for a particular input

optical power, due to the electronic feedback, then there should be two corresponding output distributions. It should therefore be possible to find a device length which can produce either a crossed or a bar state at one value of incident power depending on the previous condition. This could have applications in optical memory devices since the coupler "remembers" its previous state. The bistability may also be advantageous for optical communications since the signal power could be kept constant and the switching controlled by a single high or low pulse.

The bistability was observed in the SEED directional coupler by varying the input optical power with an acousto-optic modulator and then plotting the output power from the upper waveguide versus the incident power. The output waveforms from the signal generator, acousto-optic modulator, and the upper waveguide of the coupler, are shown in figure 25. The bistability can be observed in the latter waveform since the slope of the distorted triangle wave is different on the rising edge than it is on the falling edge.

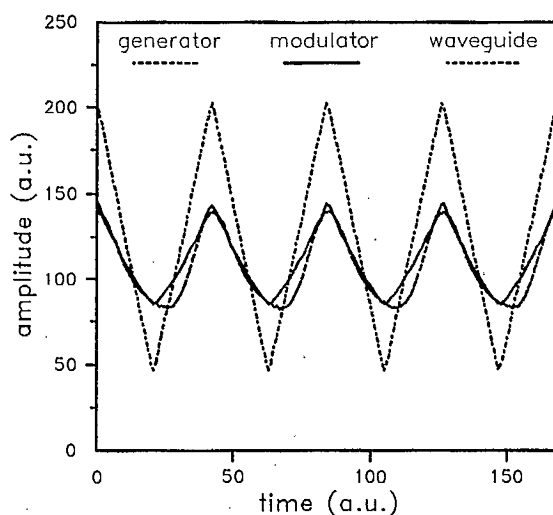

Fig. 25 Waveforms from the signal generator, acousto-optic modulator, and photodetector. The distorted waveform from the detector indicates bistability in the coupler.

The bistability can be seen more clearly from the hysteresis loop shown in figure 26. This was obtained by plotting the output power from the waveguide on the y-axis versus the power from the AOM on the x-axis.

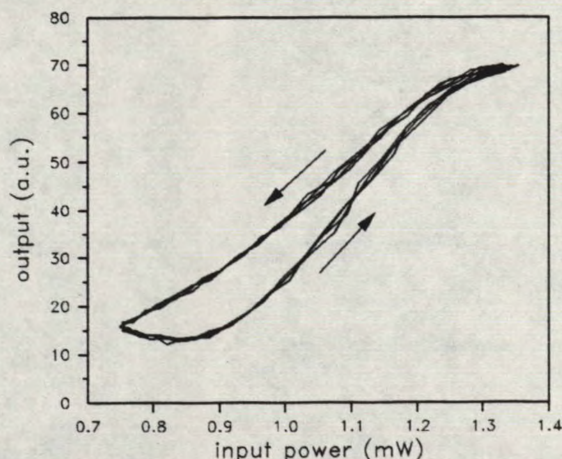

Fig. 26 Hysteresis loop obtained by plotting optical output from the upper waveguide versus optical input power.

Conclusions

The MQW-coupled, pin-doped vertical directional coupler is a highly versatile and promising device for future optical systems. We have concentrated here on the electrooptic switching capabilities of the coupler which are attributed to the quantum-confined Stark effect. Promising experimental results have been obtained with control voltages in the range of 5-10 V. These bias levels were shown to be sufficient to achieve almost complete switching for sample lengths of 300-400μm.

A theoretical model was used to show a good agreement with measured parameters. This model used the resonant tunneling technique to compute the exciton resonance wavelengths and oscillator strengths and then produced the absorption spectra of the MQW under various electric fields. The Kramers-Kronig relation was then used to translate changes in absorption to changes in refractive index and ultimately, into changes in cross-coupling between the two waveguides of the device.

The speed of the device is expected to be limited by the capacitance of the structure which can be reduced by decreasing the surface area of the electrical contacts. For optimum performance the coupler should be redesigned to use channel waveguides. The fundamental limit is determined by the speed at which the electron wave function can respond or in other words the time required for the electrons and holes to be pulled to opposite sides of the wells. This is estimated to be approximately one picosecond.

Operation of the multiple quantum well vertical directional coupler as a self-electrooptic effect device has also been demonstrated. A simple arrangement with only a single external resistor and voltage source was employed. This configuration exhibits good flexibility in that the optical powers required for switching can be adjusted by the size of the resistor and variations in source wavelength can be compensated by the bias voltage. A high contrast switching operation was achieved with constant output power. This could be beneficial when detecting the signal from each waveguide since the constant output power would produce an equal signal-to-noise ratio at each detector. Evidence of optical bistability was also reported but requires further investigation.

References

[1] B.P.Keyworth, M.Cada, J.M.Glinski, A.J.SpringThorpe, P.Mandeville, "All-Optical Switching in a GaAs-Based MQW Directional Coupler", Canadian J. Physics, vol. 67, p.408, (1989).

[2] M.Cada, B.P.Keyworth, J.M.Glinski, C.Rolland, A.J.SpringThorpe, K.O.Hill, R.A.Soref, "Electrooptical Switching in a GaAs Multiple Quantum Well Directional Coupler", Appl. Phys. Lett., vol. 54 (25), p.2509, (1989).

[3] M.Cada, B.P.Keyworth, J.M.Glinski, C.Rolland, A.J.SpringThorpe, C.J.Miner, K.O.Hill, "Two-Wavelength Optical Switching in a GaAs Multiple Quantum Well Directional Coupler", Appl. Phys. Lett., vol. 56 (21), (1990).

[4] M.Cada, B.P.Keyworth, J.M.Glinski, A.J.SpringThorpe, C.Rolland, K.O.Hill, "Electrooptic Switching in a p-i-n Doped MQW Directional Coupler", accepted for publication, J. Appl. Phys., (1990).

[5] D.A.B.Miller, D.S.Chemla, T.C.Damen, A.C.Gossard, W.Wiegmann, T.H.Wood, C.A.Burrus, "Novel hybrid optically bistable switch: The quantum well self-electro-optic effect device", Appl. Phys. Lett., vol. 45, p.13, (1984).

[6] L.Esaki and R.Tsu, "Superlattice and Negative Conductivity in Semiconductors", IBM Res. Note, RC-2418, Mar. 1969.

[7] S.Wabnitz, E.M.Wright, C.T.Seaton, G.I.Stegeman, "Instabilities and all-optical phase-controlled switching in a nonlinear directional coherent coupler", Appl. Phys. Lett., vol. 49 (14), p.838, 1986.

[8] P. Li Kam Wa and P.N.Robson, "Optical Nonlinearities in a Passive GaAs/AlGaAs Multiple Quantum Well Strain-Induced Waveguide", IEEE J. Quantum Electron., vol. QE-23 (11), p.1962, 1987.

[9] T.Y.Hsu, W.Y.Wu, U.Efron, "Amplitude and Phase Modulation in a 4 μm-thick GaAs/AlGaAs Multiple Quantum Well Modulator", Electronics Letters, vol. 24 (10), p.603, 1988.

[10]T.H.Wood, C.A.Burrus, R.S.Tucker, J.S.Weiner, D.A.B.Miller, D.S.Chemla, T.C.Damen, A.C.Gossard, W.Weigmann, "100 ps Waveguide Multiple Quantum Well (MQW) Optical Modulator with 10:1 ON/OFF Ratio", Electronic Letters, vol. 21, p.693, 1985.

[11]A.Ajisawa, M.Fujiwara, J.Shimuzu, M.Sugimoto, M. Uchida, Y.Ohta, "Monolithically Integrated Optical Gate 2x2 Matrix Switch Using GaAs/AlGaAs Multiple Quantum Well Structure", Electronics Letters, vol. 23 (21), p.1121, 1987.

[12]J.E.Zucker, T.L.Hendrickson, C.A.Burrus, "Low-Voltage Phase Modulation in GaAs/AlGaAs Quantum Well Optical Waveguides", Electronics Letters, vol. 24 (2), p.112, 1988.

[13]B.F.Levine, C.G.Bethea, G.Hasnain, J.Walker, R.J.Malik, "GaAs/Al-GaAs Quantum-Well, Long-Wavelength Infra-Red (LWIR) Detector With A Detectivity Comparable To HgCdTe", Electronics Letters, vol. 24 (12), p.747, 1988.

[14]C.R.Giles, T.Li, T.H.Wood, C.A.Burrus, D.A.B.Miller, "All-Optical Regenerator", Electronics Letters, vol. 24 (14), p.848, 1988.

[15]Y.Kawamura, K.Wakita, Y.Yoshikuni, Y.Itaya, H.Asahi, "Monolithic Integration of a DFB Laser and an MQW Optical Modulator in the 1.5 μm Wavelength Range", IEEE J. Quantum Electron., vol. QE-23 (6), p.915, 1987.

[16]H.Sakaki, H.Kurata, M.Yamanishi, "Novel Quantum-Well Optical Bistabilty Device With Excellent ON/OFF Ratio And High Speed Capability", Electronics Letters, vol. 24 (1), p.1, 1988.

[17]S.Adachi, "GaAs, AlAs, and $Al_xGa_{1-x}As$: Material parameters for use in research and device applications", J. Appl. Phys., vol. 58 (3), p.R1, 1985.

[18]L.Esaki, "A Bird's-Eye View on the Evolution of Semiconductor Superlattices and Quantum Wells", IEEE J. Quantum Electron., vol, QE-22 (9), p.1611, 1986.

[19]P.J.Stevens, M.Whitehead, G.Parry, K.Woodbridge, "Computer Modelling of the Electric Field Dependent Absorption Spectrum of Multiple Quantum Well Material", IEEE J. Quantum Electron., vol. 24 (10), p.2007, 1988.

[20]A.Harwit, J.S.Harris,Jr., A.Kapitulnik, "Calculated quasi-eigenenergies of quantum well superlattices in an applied electric field", J. Appl. Phys., vol. 60 (9), p.3211, 1986.

[21]D.A.B.Miller, D.S.Chemla, T.C.Damen, A.C.Gossard, W.Wiegmann, T.H.Wood, C.A.Burrus, "Electric field dependence of optical absorption near the bandgap of quantum-well structures", Phys. Rev. B, vol. 32 (2), p.1043, 1985.

[22]D.A.B.Miller, J.S.Weiner, D.S.Chemla, "Electric-Field Dependence of Linear Optical Properties in Quantum Well Structures: Waveguide Electroabsorption and Sum Rules", IEEE J. Quantum Electron., vol. QE-22 (9), p.1816, 1986.

[23]S.W.Koch, N.Peyghambarian, H.M.Gibbs, "Band-edge nonlinearities in direct-gap semiconductors and their application to optical bistability and optical computing", J. Appl. Phys., vol. 63 (2), p.R1, 1988.

[24]D.S.Chemla, D.A.B.Miller, P.W.Smith, "Nonlinear optical properties of GaAs/AlGaAs multiple quantum well material: phenomena and applications", Optical Eng., vol. 24 (4), p.556, 1985.

[25]A.Yariv, "Coupled-Mode Theory for Guided-Wave Optics", IEEE J.Quantum Electron., vol. QE-9 (9), p.919, 1973.

[26]D.S.Chemla, D.A.B.Miller, P.W.Smith, A.C.Gossard, W.Weigmann, "Room Temperature Excitonic Nonlinear Absorption and Refraction in GaAs/AlGaAs Multiple Quantum Well Structures", IEEE J. Quantum Electron., vol. QE-20 (3), p.265, 1984.

[27]M.D.A.MacBean, O.Mikami, C.D.W.Wilkinson, P.Mistry, J.S.Roberts, "Optical properties of (Al,Ga)As/GaAs multiple quantum well planar waveguides and the fabrication of single-mode rib waveguides and directional couplers by reactive ion etching", Applied Physics, vol. 26 (13), p.2625, 1987.

Appendix A

```
**************************************************************************
*                                                                        *
*                         Program : MODEL.BAS                            *
*                     Written by: BARRIE P. KEYWORTH                     *
*                         Date : September, 1990                         *
*                                                                        *
*       This program may be used to analyze the electrooptic switching   *
*       characteristics of multiple quantum well directional couplers.   *
*       The program is set up for use with GaAs based MQWs but can be    *
*       easily modified to work for InP.  The parameters of the MQW are  *
*       specified at the beginning of the program.                       *
*                                                                        *
*       Note:  This is a working program but is still under development. *
*       It is recommended for use with QUICK BASIC which uses a coprocessor *
*       chip.  Subroutines have been avoided in this program since they  *
*       slow down the computations.                                      *
*                                                                        *
**************************************************************************

    DIM DAT(250), DAT2(250), ZDAT(250), DIF(250), REF(250), HW(250),
    DIM V1(210), V2(210), K#(3, 210), M#(3,210),F#(3,210),FPRIME#(3 210),
    DIM TRANS#(3, 210), A#(3, 210),ENERGY#(4), EN#(4), MIN(4), MAX(4),
    DIM SIGN(4), FMAX(3), NM(3), ZREF(250), ZDIF(250),BETA(10),
    DIM LENGTHS(110,2),DISPEQ(110),INDEX(110, 2), CROSS(110, 2), WAV(250)
  DEF FNHH (NBETA) = SQR(NG ^ 2 - NBETA ^ 2)
  DEF FNQQ (NBETA) = SQR(NBETA ^ 2 - NB ^ 2)
  DEF FNPP (NBETA, NM) = SQR(NBETA ^ 2 - NM ^ 2)
  DEF FNDISP (HH,P,Q,KO) = TAN(KO*HH*TG)*HH*(1-P*Q / HH ^ 2) - P - Q
  DEF FNSPEC (HW) = AH * EXP(-(HW - HWHH) ^ 2 / (HGH ^ 2 * 2)) + AL *
                    EXP(-(HW - HWLH) ^ 2 / (HGL ^ 2 * 2)) + 2 * AC /
                    ((1 + EXP((HWC - HW) / HGC)) * (1 + EXP(-2 * PI *
                    (ABS(HWC - HW) / RY) ^ -.5)))
  DEF FNSPECO (HW) = 2 * AC / ((1 + EXP((HWZ - HW) / HGZ)) * (1 + EXP(-2*
                    PI * (ABS(HWZ - HW) / RY) ^ -.5)))
  DEF FNCOSH (X) = (EXP(X) + EXP(-X)) / 2!
  DEF FNSINH (X) = (EXP(X) - EXP(-X)) / 2!
  PI = 3.1415927#
  MO# = 9.109E-31                         'MASS OF ELECTRON IN Kg
  STYLE% = &H8000
  RY = .0042
  BIAS = 0!
  TI = .000001      ' THICKNESS OF INTRINSIC LAYER
  LZ = 1E-08        ' THICKNESS OF WELLS
  LB = 1E-08        ' THICKNESS OF BARRIERS FOR ENERGY CALCULATIONS
  TB = 2.1E-08       ' TRUE THICKNESS OF BARRIERS
```

```
X = .33             ' Al CONCENTRATION,  0.32  FOR OUR DESIGN
NPTS1% = 210        ' NUMBER OF POTENTIAL STEPS
NPTS2% = 20         ' NUMBER OF ENERGY STEPS

MBE# = (.0665 + .0835 * X) * MO#
MBHH# = (.34 + .412 * X) * MO#                          ' EFFECTIVE MASS
MBLH# = (.094 + .066 * X) * MO#
ME# = (.0665) * MO#
MHH# = (.34) * MO#                           ' EFFECTIVE MASS
MLH# = (.094) * MO#
EG1 = 1.424                                     ' BANDGAP GaAs
IF X < .45 THEN
 EG2 = 1.424 + 1.247 * X
ELSE
 EG2 = 1.9 + .125 * X + .143 * X ^ 2            'BANDGAP AlGaAs
END IF
EV = (EG2 - EG1) * .43              'VALENCE BAND POTENTIAL (60:40)
EC = (EG2 - EG1) * .57              'CONDUCTION BAND POTENTIAL
H# = 6.63E-34 / (2 * PI)            ' H-tick
DELZ# = (LZ + 2 * LB) / (NPTS1% - 1)
CLS
100     VSTEP# = (BIAS / TI) * DELZ#
VZ = 0
VB = EV
CZ = 0
CB = EC
FOR I = 1 TO NPTS1%
 Z = (I - 1) * DELZ#
 IF Z > LB AND Z < (LB + LZ) THEN
  V1(I) = CZ
  V2(I) = VZ
 ELSE
  V1(I) = CB
  V2(I) = VB
 END IF
 VZ = VZ - VSTEP#
 VB = VB - VSTEP#
 CZ = CZ + VSTEP#
 CB = CB + VSTEP#
NEXT I
IMIN = INT((LB) / DELZ#) + 4
E1MIN = V1(INT(.8 * NPTS1% / 2)) + EC * .01
E2MIN = V2(INT(1.2 * NPTS1% / 2)) + EV * .005
E3MIN = V2(INT(NPTS1% / 2)) + EV * .01
E1MAX = E1MIN + EC - VSTEP# * 4
E2MAX = E2MIN + EV - VSTEP# * 4
E3MAX = E3MIN + EV - VSTEP# * 4
 MIN(1) = 1E+20
 MIN(2) = 1E+20
```

```
          MIN(3) = 1E+20
         FOR I = 1 TO 3
         FOR N = 1 TO NPTS2%
          E1# = E1MIN + ((E1MAX - E1MIN) * (N - 1) / (NPTS2% * 3!))
          E2# = E2MIN + ((E2MAX - E2MIN) * (N - 1) / (NPTS2% * 3!))
          E3# = E3MIN + ((E3MAX - E3MIN) * (N - 1) / (NPTS2% * 3!))
          FOR J = 1 TO NPTS1%
           K#(1, J) = (SQR((2 * ABS(1.6E-19 * (E1# - V1(J))))) / H#) * SQR(ME#)
           K#(2, J) = (SQR((2 * ABS(1.6E-19 * (E2# - V2(J))))) / H#) * SQR(MHH#)
           K#(3, J) = (SQR((2 * ABS(1.6E-19 * (E3# - V2(J))))) / H#) * SQR(MLH#)
           IF (DELZ# * (J - 1)) > LB AND (DELZ# * (J - 1)) < (LB + LW) THEN
            M#(1, J) = ME#
            M#(2, J) = MHH#
            M#(3, J) = MLH#
           ELSE
            M#(1, J) = MBE#
            M#(2, J) = MBHH#
            M#(3, J) = MBLH#
           END IF
          NEXT J
          F#(I, NPTS1%) = 1!
          FPRIME#(I, NPTS1%) = 0!
           FOR J = NPTS1% - 1 TO 1 STEP -1
            ARG = -K#(I, J + 1) * DELZ#
            SIGN(1) = E1# - V1(J)
            SIGN(2) = E2# - V2(J)
            SIGN(3) = E3# - V2(J)
            IF (SIGN(I)) > 0 THEN
             F#(I,J) = COS(ARG)*F#(I,J+1)+SIN(ARG)*FPRIME#(I,J+1)/K#(I, J + 1)
             FPRIME#(I, J) = -(K#(I,J+1)*M#(I,J)/M#(I,J+1))*SIN(ARG)*F#(I,J+1)+
                             COS(ARG)*M#(I,J)*FPRIME#(I, J + 1) / M#(I, J + 1)
            ELSE
             F#(I,J)=FNCOSH(ARG)*F#(I,J+1)+FNSINH(ARG)*FPRIME#(I,J+1)/K#(I,J+1)
             FPRIME#(I,J)=(K#(I,J+1)*M#(I, J)/M#(I,J+1))*FNSINH(ARG)*F#(I,J+1)+
                          FNCOSH(ARG)*M#(I,J)*FPRIME#(I,J+1)/M#(I,J+1)
            END IF
           NEXT J
           TRANS#(I,N)=F#(I, 1) - 1
           IF N > 2 THEN
            TSIGN = TRANS#(I, N) - TRANS#(I, N - 1)
            OLDSIGN = TRANS#(I, N - 1) - TRANS#(I, N - 2)
            EN#(1) = E1#
            EN#(2) = E2#
            EN#(3) = E3#
REM         IF TSIGN > 0 AND OLDSIGN < 0 THEN 200
            IF TRANS#(I, N) * TRANS#(I, N - 1) < 0 THEN
             EHIGH# = EN#(I)
             ELOW# = ENERGY#(I)
             OLDEMID# = 0
```

```
150         EMID# = (EHIGH# + ELOW#) / 2!
            E1# = EMID#
            E2# = EMID#
            E3# = EMID#
            FOR J = 1 TO NPTS1%
             K#(1,J)= SQR((2 * ABS(1.6E-19 * (E1# - V1(J))))) / H#) * SQR(ME#)
             K#(2,J)=(SQR((2 * ABS(1.6E-19 * (E2# - V2(J))))) / H#) * SQR(MHH#)
             K#(3,J)=(SQR((2 * ABS(1.6E-19 * (E3# - V2(J))))) / H#) * SQR(MLH#)
             IF (DELZ# * (J - 1)) > LB AND (DELZ# * (J - 1)) < (LB + LW) THEN
              M#(1, J) = ME#
              M#(2, J) = MHH#
              M#(3, J) = MLH#
             ELSE
              M#(1, J) = MBE#
              M#(2, J) = MBHH#
              M#(3, J) = MBLH#
             END IF
            NEXT J
            FOR II = 1 TO 3
            F#(II, NPTS1%) = 1!
            FPRIME#(II, NPTS1%) = 0!
             FOR J = NPTS1% - 1 TO 1 STEP -1
              ARG = -K#(II, J + 1) * DELZ#
              SIGN(1) = E1# - V1(J)
              SIGN(2) = E2# - V2(J)
              SIGN(3) = E3# - V2(J)
                IF (SIGN(II)) > 0 THEN
         F#(II,J) = COS(ARG)*F#(II,J+1)+SIN(ARG)*FPRIME#(II,J+1)/K#(II,J+1)
         FPRIME#(II,J)=-(K#(II,J+1)*M#(II,J)/M#(II,J+1))*SIN(ARG)*F#(II,J+1)
                           +COS(ARG)*M#(II,J)*FPRIME#(II, J + 1) / M#(II, J + 1)
             ELSE
         F#(II,J)=FNCOSH(ARG)*F#(II,J+1)+FNSINH(ARG)*FPRIME#(II,J+1)/K#(II,J+1)
         FPRIME#(II,J)=(K#(II,J+1)*M#(II, J)/M#(II,J+1))*FNSINH(ARG)*F#(II,J+1)
                         +FNCOSH(ARG)*M#(II,J)*FPRIME#(II,J+1)/M#(II,J+1)
             END IF
             NEXT J
            NEXT II
            TRAN# = F#(I, 1) - 1
            IF TRANS#(I, N) * TRAN# < 0! THEN
             ELOW# = EMID#
             TRANS#(I, N - 1) = TRAN#
            ELSE
             EHIGH# = EMID#
             TRANS#(I, N) = TRAN#
            END IF
            EDIF# = EMID# - OLDEMID#
            IF ABS(TRAN#) > 100 AND ABS(EDIF#) > .000000000001# THEN
             OLDEMID# = EMID#
             GOTO 150
```

```
          END IF
          ENERGY#(I) = EMID#
          GOTO 200
         END IF
         IF ABS(TRANS#(I, N)) < MIN(I) THEN
          MIN(I) = ABS(TRANS#(I, N))
          ENERGY#(I) = EN#(I)
         END IF
        END IF
        NEXT N
200    NEXT I
        STRNHH = 0!
        STRNLH = .0045
          BINDHH=.007
          BINDLH=.008
    HWHH=EG1+(ENERGY#(1)-V1(NPTS1%/2))+(ENERGY#(2)-V2(NPTS1%/2))-STRNHH-BINDHH
    HWLH=EG1+(ENERGY#(1)-V1(NPTS1%/2))+(ENERGY#(3)-V2(NPTS1%/2))-STRNLH-BINDLH
        IF BIAS = 0 THEN
         HWC = HWLH
        END IF
REM       PRINT "BIAS="; BIAS; "  HH PEAK: "; HWHH; "   LH PEAK: "; HWLH
REM       INPUT DUM$
        E1# = ENERGY#(1)
        E2# = ENERGY#(2)
        E3# = ENERGY#(3)
        FOR J = 1 TO NPTS1%
         K#(1, J) = (SQR((2 * ABS(1.6E-19 * (E1# - V1(J))))) / H#) * SQR(ME#)
         K#(2, J) = (SQR((2 * ABS(1.6E-19 * (E2# - V2(J))))) / H#) * SQR(MHH#)
         K#(3, J) = (SQR((2 * ABS(1.6E-19 * (E3# - V2(J))))) / H#) * SQR(MLH#)
         IF (DELZ# * (J - 1)) > LB AND (DELZ# * (J - 1)) < (LB + LW) THEN
          M#(1, J) = ME#
          M#(2, J) = MHH#
          M#(3, J) = MLH#
         ELSE
          M#(1, J) = MBE#
          M#(2, J) = MBHH#
          M#(3, J) = MBLH#
         END IF
        NEXT J
        FOR I = 1 TO 3
        F#(I, NPTS1%) = 1!
        FPRIME#(I, NPTS1%) = 0!
         FOR J = NPTS1% - 1 TO 1 STEP -1
          ARG = -K#(I, J + 1) * DELZ#
          SIGN(1) = E1# - V1(J)
          SIGN(2) = E2# - V2(J)
          SIGN(3) = E3# - V2(J)
          IF (SIGN(I)) > 0 THEN
```

```
    F#(I,J) = COS(ARG)*F#(I,J+1)+SIN(ARG)*FPRIME#(I,J+1)/K#(I, J + 1)
    FPRIME#(I, J) = -(K#(I,J+1)*M#(I,J)/M#(I,J+1))*SIN(ARG)*F#(I,J+1)+
                    COS(ARG)*M#(I,J)*FPRIME#(I, J + 1) / M#(I, J + 1)
   ELSE
    F#(I,J)=FNCOSH(ARG)*F#(I,J+1)+FNSINH(ARG)*FPRIME#(I,J+1)/K#(I,J+1)
    FPRIME#(I,J)=(K#(I,J+1)*M#(I, J)/M#(I,J+1))*FNSINH(ARG)*F#(I,J+1)+
                 FNCOSH(ARG)*M#(I,J)*FPRIME#(I,J+1)/M#(I,J+1)
   END IF
  NEXT J
 NEXT I
FOR I = 1 TO 3
 FOR J = NPTS1% - 2 TO 1 STEP -1
  OLDSLOPE = F#(I, J + 1) - F#(I, J + 2)
  SLOPE = F#(I, J) - F#(I, J + 1)
  IF OLDSLOPE > 0 AND SLOPE < 0 THEN
   FMAX(I) = F#(I, J + 1)
  END IF
  IF (OLDSLOPE < 0 AND SLOPE > 0) OR F#(I, J) < 1 THEN
   FOR K = J TO 1 STEP -1
    F#(I, K) = 1
   NEXT K
   GOTO 300
  END IF
 NEXT J
300     NEXT I
OVERLAP1 = 0
OVERLAP2 = 0
SUM1 = 0
SUM2 = 0
SUM3 = 0
FOR I = 1 TO NPTS1%
 FOR J = 1 TO 3
  F#(J, I) = F#(J, I) - 1          ' SINCE WE START WITH f#(N)=1
 NEXT J
 SUM1 = F#(1, I) ^ 2 + SUM1
 SUM2 = F#(2, I) ^ 2 + SUM2
 SUM3 = F#(3, I) ^ 2 + SUM3
NEXT I
SCALE1 = 1 / (DELZ# * SUM1)
SCALE2 = 1 / (DELZ# * SUM2)
SCALE3 = 1 / (DELZ# * SUM3)
FOR I = 1 TO NPTS1%
 F#(1, I) = F#(1, I) * SQR(SCALE1)
 F#(2, I) = F#(2, I) * SQR(SCALE2)
 F#(3, I) = F#(3, I) * SQR(SCALE3)
 OVERLAP1 = F#(1, I) * F#(2, I) + OVERLAP1
 OVERLAP2 = F#(1, I) * F#(3, I) + OVERLAP2
NEXT I
IF BIAS = 0 THEN
```

```
 OLAP1 = OVERLAP1
 OLAP2 = OVERLAP2
 HWZ = HWHH
END IF
OVERLAP1 = (OVERLAP1 / OLAP1) ^ 2
OVERLAP2 = (OVERLAP2 / OLAP2) ^ 2
H = 6.63E-34 / (2 * PI * 1.6E-19)       ' CHANGES h TO WORK IN eV
HGH = .003 + BIAS ^ 2 * .00004
HGL = .003 + BIAS ^ 2 * .00004
HGC = .005 + BIAS ^ 2 * .00004
AH = 11.5 * OVERLAP1
AL = 6! * OVERLAP2
AC = 3.8
IF BIAS <> 0 THEN 600
HW(1) = 1.42
FOR I = 1 TO 100
 DAT(I) = FNSPEC(HW(I))
 HW(I + 1) = HW(I) + (1.5 - 1.42) / 99!
 WAV(I) = 3 * 6.63E-17 / (HW(I) * 1.6E-19)       ' WAVELENGTH IN nm '
NEXT I
CLS
SCREEN 9
VIEW (100, 26)-(600, 256), , 1
WINDOW (820, 0)-(880, 14)
VIEW PRINT 1 TO 3
PRINT TAB(30); "    ABSORPTION SPECTRUM"
PRINT "  14.0"
VIEW PRINT 11 TO 12
PRINT "      "
FOR I = 1 TO 5
 TICK = 820 + I * 10
 LINE (TICK, 0)-(TICK, .3)
 LINE (TICK, 14)-(TICK, 13.7)
NEXT I
FOR I = 1 TO 6
 TICK = 815 + I * 10
 LINE (TICK, 0)-(TICK, .2)
 LINE (TICK, 14)-(TICK, 13.8)
NEXT I
FOR I = 2 TO 100
LINE (WAV(I - 1), DAT(I - 1))-(WAV(I), DAT(I))
NEXT I
VIEW PRINT 19 TO 21
PRINT "   0.0"
PRINT TAB(10); "820"; TAB(36); "WAVELENGTH (nm) "; TAB(75); "880"
VIEW PRINT 22 TO 23
PRINT TAB(25);
600     INPUT "OUTPUT WAVEFUNCTION TO FILE (Y or N) "; ANS$
IF ANS$ = "N" OR ANS$ = "n" THEN 650
```

```
        PRINT
        PRINT TAB(30);
        INPUT "ENTER FILENAME (.DAT)"; NAM2$
        OPEN NAM2$ FOR OUTPUT AS #1
        FOR I = 1 TO NPTS1%
         W1! = F#(1, I)
         W2! = F#(2, I)
         W3! = F#(3, I)
         PRINT #1, (I - 1) * DELZ# * 1E+09; W1!; W2!; W3!
        NEXT I
        PRINT #1, OVERLAP1; OVERLAP2
        CLOSE #1
650     IF BIAS = 0 THEN
         PRINT
         PRINT TAB(33);
         INPUT "ENTER BIAS VOLTAGE "; BIAS
         GOTO 100
        END IF
        FOR I = 1 TO 100
        DAT2(I) = FNSPEC(HW(I))
        NEXT I
        FOR I = 2 TO 100
        LINE (WAV(I - 1), DAT2(I - 1))-(WAV(I), DAT2(I)), , , STYLE%
        NEXT I
        PRINT : PRINT TAB(20);
        INPUT "Q TO QUIT, Y TO RESTART, ENTER TO CONTINUE "; ANS$
        IF ANS$ = "Y" OR ANS$ = "y" THEN
         PRINT TAB(33);
         INPUT "ENTER BIAS VOLTAGE "; BIAS
         GOTO 100
        END IF
        IF ANS$ = "q" OR ANS$ = "Q" THEN 999
        CLS
        SCALE = 3E+08 * .0008 * H * 5000000! / PI' SCALE BY 50
        FOR I = 1 TO 100
        DIF(I) = DAT2(I) - DAT(I)
        NEXT I
        FOR I = 1 TO 100
         REF(I) = 0
         FOR J = 1 TO I - 1
         REF(I) = DIF(J) / (HW(J) ^ 2 - HW(I) ^ 2) + REF(I)
         NEXT J
         FOR J = I + 1 TO 100
         REF(I) = DIF(J) / (HW(J) ^ 2 - HW(I) ^ 2) + REF(I)
         NEXT J
         REF(I) = REF(I) * SCALE
         NEXT I
        MAX = 0
        FOR I = 1 TO 100
```

```
 DIFF = MAX - ABS(DIF(I))
 IF DIFF < 0 THEN MAX = ABS(DIF(I))
 DIFF = MAX - ABS(REF(I))
 IF DIFF < 0 THEN MAX = ABS(REF(I))
NEXT I
MAX = INT(MAX + 1)
VIEW (100, 26)-(600, 256), , 1
WINDOW (820, -MAX)-(880, MAX)
VIEW PRINT 1 TO 3
PRINT TAB(30); "  DIFFERENTIAL SPECTRUM        "
PRINT " +"; MAX; "   "
LINE (820, 0)-(880, 0)
VIEW PRINT 11 TO 12
PRINT "   0.0"
FOR I = 2 TO 100
LINE (WAV(I - 1), DIF(I - 1))-(WAV(I), DIF(I))
LINE (WAV(I - 1), REF(I - 1))-(WAV(I), REF(I)), , , STYLE%
NEXT I
VIEW PRINT 19 TO 21
PRINT " -"; MAX; "   "
PRINT TAB(10); "820"; TAB(36); "WAVELENGTH (nm) "; TAB(75); "880"
VIEW PRINT 22 TO 23
PRINT : PRINT : PRINT TAB(35);
INPUT "RESTART (Y or N) "; ANS$
IF ANS$ = "Y" OR ANS$ = "y" THEN
 BIAS = 0
 GOTO 100
END IF

' CALCULATE THE COUPLING VERSUS WAVELENGTH '

SLENGTH = .3       ' SAMPLE LENGTH IN mm '
NB = 3.36272
NG = 3.56539
TM = .0000009
TG = .0000018
GOSUB 2000             ' CALCULATE ZERO BIAS REFRACTIVE INDEX BY
PRINT                  ' ADDING EXCITONIC AND BACKGROUND TERMS
CLS
SCREEN 0
PRINT TAB(30); : PRINT "WORKING !"
FOR J = 1 TO 2
FOR I = 1 TO 100
NM(1) = INDEX(I, 1)
NM(2) = INDEX(I, 1) + REF(I) / 50!
INC = (NG - NM(J)) / 50!
IF NM(J) > 3.562 THEN
 CROSS(I, J) = 100
 L = 0
```

```
         PRINT " TOO HIGH"
         GOTO 900
        END IF
        BMAX = NG - INC * 3
        BMIN = NM(J) + INC
        NBETA = BMAX
        LAMBDA = 3 * 6.63E-26 / (HW(I) * 1.6E-19)
        PI = 3.14159
        KO = 2 * PI / LAMBDA
        NM = NM(J)
        HH = FNHH(NBETA)
        P = FNPP(NBETA, NM)
        Q = FNQQ(NBETA)
        OLDDIFF = FNDISP(HH, P, Q, KO)
        OLDSLOPE = 0#

700     WHILE NBETA > BMIN
        NBETA = NBETA - INC
        HH = FNHH(NBETA)
        P = FNPP(NBETA, NM)
        Q = FNQQ(NBETA)
        DIFF = FNDISP(HH, P, Q, KO)
REM     PRINT "NBETA = "; NBETA; "  DIFF = "; DIFF; "  INC = "; INC
        SLOPE = DIFF - OLDDIFF
        SIGN = OLDDIFF * DIFF
        DIP = SLOPE * OLDSLOPE
        IF SIGN < 0! OR DIP < 0! THEN
        IF ABS(DIFF) < .05 THEN
REM     PRINT "NORMALIZED BETA = "; NBETA; "  DIFF = "; DIFF
        INC = (NG - NM(J)) / 50!
        BETA = NBETA
        OLDSLOPE = SLOPE
        OLDDIFF = DIFF
        GOTO 800
        ELSEIF ABS(DIFF) > 1000! THEN
        INC = (NG - NM(J)) / 50!
        NBETA = NBETA - INC
        HH = FNHH(NBETA)
        P = FNPP(NBETA, NM)
        Q = FNQQ(NBETA)
        OLDDIFF = FNDISP(HH, P, Q, KO)
        OLDSLOPE = 0!
        ELSE
         NBETA = NBETA + INC
         INC = INC / 50!
         IF INC < .000001 THEN
          INC = (NG - NM(J)) / 50!
          NBETA = NBETA - INC * 2
          HH = FNHH(NBETA)
```

```
      P = FNPP(NBETA, NM)
      Q = FNQQ(NBETA)
      OLDDIFF = FNDISP(HH, P, Q, K0)
      OLDSLOPE = 0!
     END IF
    END IF
    GOTO 700
    END IF
    OLDSLOPE = SLOPE
    OLDDIFF = DIFF
    WEND
800 NBETA = BETA
    IF NBETA < BMIN + INC THEN
     PRINT : PRINT "                    ****   CRASHED   ****"
     GOTO 999
    END IF
    HH = FNHH(NBETA) * K0
    Q = FNQQ(NBETA) * K0
    P = FNPP(NBETA, NM) * K0
    C = 2.998E+08
    KTOP = 2 * EXP(-P * TM) * P * HH ^ 2
    KBOTTOM = NBETA * K0 * (TG + 2! / P) * (HH ^ 2 + P ^ 2)
    KCOEFF = KTOP / KBOTTOM
    LENGTH = PI / (2! * KCOEFF)
    L = LENGTH * 1000!
    ASIN = 1.5708
    KAPPA = ASIN / L
    CROSS(I, J) = (SIN(KAPPA * SLENGTH) ^ 2) * 100
900 LENGTHS(I, J) = L
    INDEX(I, J) = NM(J)
    NEXT I
    NEXT J
    SCREEN 9
    CLS
    VIEW (100, 26)-(600, 256), , 1
    WINDOW (820, 0)-(880, 100)
    VIEW PRINT 1 TO 4
    PRINT TAB(30); "LINEAR CROSS-COUPLING      "
    PRINT
    LMAX = 100
    PRINT TAB(4);
    PRINT LMAX
    VIEW PRINT 11 TO 12
    PRINT TAB(3);
    PRINT "(mm)"
    FOR I = 1 TO 5
     TICK = 820 + I * 10
     LINE (TICK, 0)-(TICK, 1!)
     LINE (TICK, 100)-(TICK, 99)
```

```
NEXT I
FOR I = 1 TO 6
 TICK = 815 + I * 10
 LINE (TICK, 0)-(TICK, .6)
 LINE (TICK, 100)-(TICK, 99.4)
NEXT I
FOR I = 2 TO 100
LINE (WAV(I - 1), CROSS(I - 1, 1))-(WAV(I), CROSS(I, 1))
LINE (WAV(I - 1), CROSS(I - 1, 2))-(WAV(I), CROSS(I, 2)), , , STYLE%
NEXT I
VIEW PRINT 20 TO 24
PRINT TAB(4);
PRINT "0.0"
PRINT TAB(10); "820"; TAB(36); "WAVELENGTH (nm)  "; TAB(75); "880"
VIEW PRINT 22 TO 23
PRINT : PRINT : PRINT TAB(30);
INPUT "OUTPUT TO FILE (Y or N) "; ANS$
IF ANS$ = "Y" OR ANS$ = "y" THEN
PRINT : PRINT TAB(30);
INPUT "ENTER FILENAME (.DAT)"; NAM2$
OPEN NAM2$ FOR OUTPUT AS #1
PRINT #1,"ENERGY;WLENGTH;ALPHA1;ALPHA2;DALPHA;DINDEX;INDEX;CLENGTH;
          COUPLING"
FOR J = 1 TO 2
FOR I = 1 TO 100
IF J = 1 THEN
 REFIN = 0
ELSE
 REFIN = REF(I) / 50!
END IF
PRINT #1, HW(I); " "; WAV(I); " "; DAT(I); " "; DAT2(I); " "; DIF(I);
          " ";REFIN;" ";INDEX(I,J);" ";LENGTHS(I,J);" "; CROSS(I, J)
NEXT I
NEXT J
CLOSE #1
END IF
PRINT : PRINT
PRINT TAB(34);
INPUT "RESTART (Y or N) "; ANS$
IF ANS$ = "Y" THEN
 BIAS = 0
 CLS
 SCREEN 0
 GOTO 100
END IF
CLS
999     END
```

```
2000    HGZ = .002
        HWZ = HWZ - .005
        HW(1) = 1.42
        FOR I = 1 TO 100
         ZDAT(I) = FNSPECO(HW(I))
        NEXT I
        CLS
        SCREEN 9
        VIEW (100, 26)-(600, 256), , 1
        WINDOW (820, 0)-(880, 14)
        VIEW PRINT 1 TO 3
        PRINT TAB(30); "    SATURATED SPECTRUM    "
        PRINT "  14.0"
        VIEW PRINT 11 TO 12
        PRINT "      "
        FOR I = 1 TO 5
         TICK = 820 + I * 10
         LINE (TICK, 0)-(TICK, .3)
         LINE (TICK, 14)-(TICK, 13.7)
        NEXT I
        FOR I = 1 TO 6
         TICK = 815 + I * 10
         LINE (TICK, 0)-(TICK, .2)
         LINE (TICK, 14)-(TICK, 13.8)
        NEXT I
        FOR I = 2 TO 100
        LINE (WAV(I - 1), DAT(I - 1))-(WAV(I), DAT(I))
        LINE (WAV(I - 1), ZDAT(I - 1))-(WAV(I), ZDAT(I)), , , STYLE%
        NEXT I
        VIEW PRINT 19 TO 21
        PRINT "   0.0"
        PRINT TAB(10); "820"; TAB(36); "WAVELENGTH (nm)   "; TAB(75); "880"
        VIEW PRINT 22 TO 23
        PRINT TAB(31);
        INPUT "TYPE ENTER TO CONTINUE "; ANS$
        CLS
        SCREEN 0
        SCALE = 3E+08 * .0008 * H * 5000000! / PI' SCALE BY 50
        FOR I = 1 TO 100
        ZDIF(I) = ZDAT(I) - DAT(I)
        NEXT I
        FOR I = 1 TO 100
         ZREF(I) = 0
         FOR J = 1 TO I - 1
         ZREF(I) = ZDIF(J) / (HW(J) ^ 2 - HW(I) ^ 2) + ZREF(I)
         NEXT J
         FOR J = I + 1 TO 100
         ZREF(I) = ZDIF(J) / (HW(J) ^ 2 - HW(I) ^ 2) + ZREF(I)
         NEXT J
```

```
 ZREF(I) = ZREF(I) * SCALE
NEXT I
NW = SQR(13.18)                        ' REF. INDEX OF GaAs
NB = SQR(13.18 - 3.12 * X)             ' REF. INDEX OF AlGaAs
RMS = SQR((LZ * NW ^ 2 + TB * NB ^ 2) / (LZ + TB))
FOR I = 1 TO 100
' rms index of MQW = 3.5317 for X=.33, 9.6 nm wells, 21nm barriers
INDEX(I, 1) = RMS - ZREF(I) / 50!
NEXT I
RETURN
```

QC
176.8
O6
C346
1990

Cada, Michael
-- Final report on optical switching in a p-i-n doped multiple quantum well vertical directional coupler.

DATE DUE

CRC LIBRARY/BIBLIOTHEQUE CRC
QC176.8.O6 C346 1990
Cada, Michael.

INDUSTRY CANADA / INDUSTRIE CANADA
208848